Applied Energy 343 (2023) 121143

Contents lists available at ScienceDirect

Applied Energy

journal homepage: www.elsevier.com/locate/apenergy

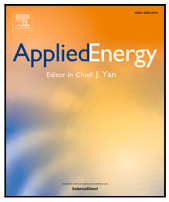

A multi-energy multi-microgrid system planning model for decarbonisation and decontamination of isolated systems

Claudio Carvallo [a], Francisca Jalil-Vega [b,c,e,*], Rodrigo Moreno [a,d,e]

[a] Departamento de Ingeniería Eléctrica, Universidad de Chile, Santiago, Chile
[b] Electrical Energy Management Group, Faculty of Engineering, University of Bristol, BS8 1UB Bristol, UK
[c] Center for Energy Transition (CENTRA), Faculty of Engineering and Sciences, Universidad Adolfo Ibáñez, Santiago, Chile
[d] Department of Electrical and Electronic Engineering, Imperial College London, London, UK
[e] Instituto Sistemas Complejos de Ingeniería, Santiago, Chile

ARTICLE INFO

Keywords:
Multi-energy systems
Multi-microgrid systems
Integrated energy systems model
Decarbonisation
Decontamination
Energy planning

ABSTRACT

Decarbonising and decontaminating remote regions in the world presents several challenges. Many of these regions feature isolation, dispersed demand in large areas, and a lack of economic resources that impede the development of robust and sustainable networks. Furthermore, isolated systems in the developing world are mostly based on diesel generation for electricity, and firewood and liquefied petroleum gas for heating, as these options do not require a significant infrastructure cost. In this context, we present a stochastic multi-energy multi-microgrid system planning model that integrates electricity, heat and hydrogen networks in isolated systems. The model is stochastic to capture uncertainty in renewable generation outputs, particularly hydro and wind, and thus design a multi-energy system proved secured against such uncertainty. The model also features two distinct constraints to limit the emissions of CO_2 (for decarbonisation) and particulate matter (for decontamination), and incorporates firewood as a heating source. Moreover, given that the focus is on low-voltage networks, we introduce a fully linear AC power flow equations set, allowing the planning model to remain tractable. The model is applied to a real-world case study to design a multi-energy multi-microgrid system in an isolated region in Chilean Patagonia. In a case with a zero limit over direct CO_2 emissions, the total system's cost increases by 34% with respect to an unconstrained case. In a case with a zero limit over particulate matter emissions, the total system's cost increases by 189%. Finally, although an absolute zero limit over both, particulate matter and direct CO_2 emissions, leads to a total system's cost increase of 650%, important benefits in terms of decarbonisation and decontamination can be achieved at marginal cost increments.

1. Introduction

As set out by the Intergovernmental Panel on Climate Change (IPCC) in its Sixth Assessment Report, it is unequivocal that human activity has caused continuous increases in greenhouse gas (GHG) concentrations, leading to unprecedented warming in the atmosphere, ocean and land. Human-induced climate change is already causing many extreme events such as heatwaves, heavy precipitation, or droughts, among others, and the IPCC has emphasised that future emissions will cause additional warming [1]. Globally, 75% of GHG emissions come from the energy sector [2]. Mitigation and adaptation measures will therefore lead to important changes in energy systems worldwide.

Additionally to decarbonising, several countries in Asia and the Global South are experiencing challenges related to reducing air pollution, specifically particulate matter PM2.5 emissions [3]. In several of these countries, PM2.5 emissions are associated to intensive use of firewood and contaminating biomass for heating and cooking purposes. One of such countries is Chile, for which biomass supplies 38% of its residential total energy demand, mostly via combustion of firewood for heating [4]. Chile declared two mitigation contributions in its updated Nationally Determined Contributions (NDC) [5]: First, meeting a carbon budget and reaching net-zero carbon emissions by 2050. Second, reducing its black carbon emissions (PM2.5) by 25% with respect to 2016 levels over the next decade. For Chile – as well as for many other Global South and Asian countries – PM2.5 reduction targets imply that the use of biomass for heating needs to be reduced, posing the challenge of moving away from a low-carbon resource while at the same time reducing GHG emissions.

Deep decarbonisation of the energy system is a cross-sector problem that cannot be addressed solely by focusing on decarbonising the electricity sector [6], since energy service demands such as heating

* Corresponding author at: Electrical Energy Management Group, Faculty of Engineering, University of Bristol, BS8 1UB Bristol, UK.
E-mail address: f.jalil-vega@bristol.ac.uk (F. Jalil-Vega).

https://doi.org/10.1016/j.apenergy.2023.121143
Received 31 December 2022; Received in revised form 31 March 2023; Accepted 10 April 2023
Available online 11 May 2023

have been identified as one of the main sources for GHG emissions worldwide, and for particulate matter in the aforementioned regions. In this context, while the option of electrifying heat via heat pumps can be appealing, other alternatives such as installing district heating networks supplied by low carbon technologies [7]; fuel switching to low-carbon fuels such as hydrogen [8]; or installing combined heat and power (CHP) units [9], among others, are potentially competitive solutions that can reduce the electricity infrastructure that would be required to electrify all energy service demands.

In order to find solutions that can simultaneously address both decarbonisation and decontamination goals in energy systems, planning and design frameworks that integrate multiple energy vectors and that account for the different emissions involved are necessary, taking advantage of synergies and flexibilities across vectors and sectors. In addition, the variability and uncertainty associated with renewable resources must be considered in order to obtain reliable solutions to scenarios of low availability of these resources. This work proposes such a modelling framework: It presents a two-stage stochastic optimisation mathematical model which determines the optimal investments and operations of an integrated electricity, heat and hydrogen energy system, considering different heat supply energy vectors to displace the use of contaminating fuels. The model is applied to an isolated region in the south of Chile, Chilean Patagonia, with an intense use of firewood and liquefied petroleum gas (LPG) for heating, and a high share of diesel in electricity generation. The novelty of this work is that it presents an integrated stochastic multi-energy multi-microgrid system planning model that includes a detailed representation of power flows using an AC formulation – i.e. considering both active and reactive powers to appropriately represent the physics of low voltage grids such as microgrids – and includes firewood as an energy carrier together with its associated particulate matter emissions.

1.1. Literature review

Significant progress has been made in recent years to reduce power systems' GHG emissions globally through the massive roll-out of renewable generation. However, in order to decarbonise whole-energy systems, cross-sector and cross-vector approaches are needed, since energy service demands such as heating, cooling, and transport, are still heavily reliant on fossil fuels. Heating is the largest end-use energy demand, representing around 50% of final energy consumption and 40% of carbon emissions globally [10]. In this context, multi-energy systems integration represents a pathway for deep decarbonisation of whole-energy systems [11].

Multi-energy systems are defined as those in which different energy vectors such as electricity, heat and other fuels interact in an optimal way [12]. These systems have been studied as an alternative for increasing technical, environmental and economic performance compared to classical systems in which these vectors are operated and planned separately [13]. Furthermore, the integration of different energy vectors has been proposed as an alternative to incorporate more flexibility into electrical systems [14]. For example, heat demands could potentially provide flexibility, as they are able to rapidly increase or decrease consumption without major impacts, due to thermal inertia in buildings [15]. Heat pumps and electric resistors can capitalise on free electricity from surplus renewables, as they can operate with thermal storage units to charge using free or low-cost electricity, and discharge to supply heat when electricity prices are high [16]. Distributed multi-generation systems have been proved able to provide real-time demand response from shifting heating or cooling energy [17], in a profitable way. Different models and mathematical tools have been proposed to study the integration of energy vectors using different approaches. Research ranges from the dynamic analysis of flows and interactions in integrated systems [18], through optimisation of integrated systems' operation [19], to larger-scale problems such as long-term planning of multi-energy systems [20].

In [21] a multi-temporal simulation model has been proposed for the analysis of systems integrating electricity, heat and gas networks. In this model, flow equations for the three energy vectors are represented by non-linear equations and solved simultaneously using a novel Newton–Raphson approach. The methodology is applied to a real case study of a multi-energy district system in the University of Manchester Campus. The model was proven able to very closely represent the interactions between different networks, as well as their losses.

In terms of operation optimisation studies in integrated systems, a robust operation optimisation model for smart districts with multi-energy technologies and integrated energy networks is proposed in [22]. The model is a two-stage iterative model. Its first stage consists of a mixed integer linear programme (MILP) using linear approximations of the network equations, while its second stage consists of a detailed non-linear integrated network model. The model is able to capture the system's uncertainty and evaluate its flexibility under stress conditions, determining its optimal operation. In [23] a model for the integrated management of active power and heat networks is presented, which is based on a dynamic dual-horizon AC-OPF optimal power flow that optimises the operation of different multi-energy technologies, considering active and reactive losses in the power grid and inter-temporal constraints. In the first stage, the day-ahead operation is planned with an hourly resolution, considering the daily electricity market conditions and the wind power forecast. In the second stage, operations are optimised for a 4-hour rolling horizon with a 15-minute resolution, taking into account both the short-term wind power forecast and the planned operation suggested in the previous stage. The case study considers a typical UK medium voltage distribution network. Ref. [24] propose a model for minimising operation costs of multi-energy multi-microgrid systems while taking into account carbon emission limits. The optimal strategy proposed in this work consists on a day-ahead stage where microgrids share electricity and operate individually, and an intra-day scheduling stage where operation and penalty costs are minimised sequentially for each microgrid.

Regarding long-term multi-energy systems planning studies, [25] proposes a stochastic mixed integer linear stochastic optimisation model for the planning and operation of multi-energy systems with distributed generation. The model considers the evaluation of flexibility in the investment and operation stages and is based on the use of real options financial thinking (RO Thinking). The methodology is applied to a UK-based case considering district energy systems. This model does not consider networks, formulating the problem in a uni-nodal way. [26] studies the role of *power-to-gas* and carbon capture in Belgium's decarbonisation pathways. The authors propose an optimisation model for centralised long-term planning of multi-energy systems including electricity, hydrogen, natural gas, synthetic methane and carbon dioxide. The model determines and sizes investments in generation, conversion, storage, and carbon capture technologies, minimising the cost of supplying energy demands heating, transport and industry sectors. As for [25], this model does not include a spatial representation of transport networks for the different energy carriers.

Ref. [27] presents an optimisation MILP model that minimises the cost of supplying heat and electricity to a spatially disaggregated region under a multi-period formulation. The model makes decisions about investments in gas, electricity and heat networks, along with optimal investments and operation of end-use technologies. Network infrastructure decisions consider distances both between and within zones, representing in this way the distribution networks involved. The model is applied in a UK case-study. [28] propose an extension of this model in order to study the role of hydrogen for decarbonising heat in urban areas in the UK. The extension consists on two formulations for hydrogen networks: the first through stand-alone networks, and the second via upgrading existing natural gas networks and making them suitable for hydrogen transport. In [29] a multi-energy system optimisation model is proposed to maximise investment and operational synergy in the electricity, heat and transport sectors, considering

the integration of a hydrogen system to minimise overall costs. The model was applied in a future system in Great Britain. One of this model's limitations is not considering stochastic scenarios to represent the uncertainty associated with renewable sources. A further limitation in [27–29] is that power flows are simplified to their DC formulation, without considering reactive power and voltages.

Recent studies show that hydrogen has taken a leading role when modelling multi-energy systems, due to its ability to compensate for seasonal or daily variations in renewable generation [30], its ability to integrate with a renewable power systems [31] and low-carbon transport sectors [32], or its potential ability to be stored in installed gas infrastructure [33], among others. [34], for example, propose a MILP optimisation model for the optimal design of district-scale multi-energy systems with seasonal hydrogen storage capacity. The novelty of the model is that it captures uncertainty in the input data and performs Monte Carlo simulations for a sensitivity analysis. The operation is solved for all the hours in a year, which implies high computational costs. The model, however, does not consider network flows, nor network infrastructure costs. Ref. [35] propose an integrated energy systems model, where hydrogen can be produced, stored, and used. The model uses a combination of stochastic and robust optimisation approaches. A relevant aspect of this work is that it incorporates a seasonal hydrogen storage model while reducing the time dimension of the problem using a typical days formulation. In terms of the electricity network, it incorporates a linear representation of the AC flows in the active distribution network, without considering losses. The methodology is applied on the IEEE-33 Power System test network. Finally, [36] propose an integrated model for planning an operation of multi-energy multi-microgrids, for the provision of heating, cooling, and power. The model minimises the whole-system's costs, considering bi-directional interactions between electricity and gas vectors. However, this model does not provide a detailed representation of networks, nor does it incorporate elements of uncertainty.

The revised literature shows and discusses the value of integrated planning of multi-energy systems over the planning of energy vectors treated independently. One of the most relevant challenges identified is the representation of low-voltage networks and flows, both electrical and thermal. This is critical in the case of microgrids and distribution systems. Very detailed models of the operation and dynamics of the different flows limit the models' scalability and reproducibility, given the non-linear equations involved. Further, when analysing recent models for optimal planning and operation of multi-energy and multi-microgrid systems, we identified that there is a trade-off in existing models on incorporating detailed network operational constraints versus including investment decisions. Models that incorporate fairly detailed operational constraints and stochastic scenarios do not consider decisions on investments in technologies and networks. On the other hand, optimisation models that make investment decisions treat the modelled systems either as uninodal, or include very simplified constraints for electricity networks, for example, considering DC flows or lossless AC flows. Finally, in terms of heating technologies, firewood, so far, has not been included in multi-energy and multi-microgrid system models as a thermal energy supply vector. Firewood plays a particularly prominent role in supplying heat demands in the Global South, considering its low operating costs and emission factors. However, its high air pollution indexes make its role uncertain in future decarbonisation scenarios.

1.2. Contributions of this paper

The most important contributions of this work are:

- Presenting a stochastic multi-energy multi-microgrid system model that makes investment and operation decisions for the planning and operation of integrated electricity, heat and hydrogen isolated systems. The model is stochastic to incorporate uncertainty in renewable generation outputs, designing a multi-energy system proved secured against various generation profiles of renewables.
- Representing the power flows – in the context of multi-energy system planning models – using an AC formulation, i.e. considering both active and reactive powers. This is critical to obtain realistic results in the context of low-voltage networks such as microgrids. This is made possible by, firstly, convexification and, secondly, linearisation of the power flow equations that allow the model to be written in mixed integer linear form.
- Modelling of firewood as an energy carrier for supplying thermal energy in an integrated multi-energy system model. In this work, firewood can be totally or partially replaced by means of generation and storage technologies, displacing particulate matter emissions.
- Incorporating, along with classical CO_2 emission constraints, particulate matter constraints. Hence, by adjusting the right-hand side of these constraints, different designs of the multi-energy multi-microgrid system can be obtained.

The model is then applied to a real case study of an isolated system in the Global South, particularly in the Chilean Patagonia – characterised by its intensive use of firewood for heating and high levels of particulate matter emissions which are hazardous to health – to understand the advantages of integrated planning, and assess possible decarbonisation and decontamination pathways for regions with similar characteristics.

2. Methodology

2.1. Model overview

The model proposed in this research is a two-stage stochastic optimisation model that makes investment and operating decisions to minimise the cost of supplying heating – space and hot water – and electricity energy service demands in residential and commercial sectors. Investment decisions are the capacities of primary, secondary, and end-use technologies supplying electricity, heat and hydrogen, together with network capacities required to transport and distribute each energy carrier. Operational decisions are the operation profiles of generation and storage technologies for each energy vector, for a set of stochastic scenarios. The source of uncertainty comes from hydrological and wind resource availability scenarios. Hence, the portfolio of investment decisions determined is proved secured against a range of scenarios that might occur, particularly those with small renewable energy contribution. The proposed model corresponds to a two-stage stochastic optimisation model, where uncertainty is represented through a scenario tree (particularly, a fan-like scenario tree) [37]. The model optimises investment decisions in the first stage (variables common to all scenarios) and operational decisions in the second stage (scenario-dependent variables). The scenario tree is designed by processing historical data, attempting to capture credible ranges of uncertainty to make robust investment decisions. Importantly, each scenario presents a large number of operating conditions to capture variable demand and the fluctuations of availability levels of renewable generation.

The model minimises investment and expected operating costs (including unserved energy costs) over one year and multiple scenarios. By using this temporal representation, it is possible to capture seasonalities of demands, temperatures, and primary resources in detail, while maintaining the model's tractability. The time horizon is configured through a representative day for each month of the year, with an hourly resolution, in order to capture the hourly and monthly variations of demands and renewable resources. While these days are independent and temporally decoupled from each other, the model allows for seasonal storage of hydrogen, by carrying energy from one month to the

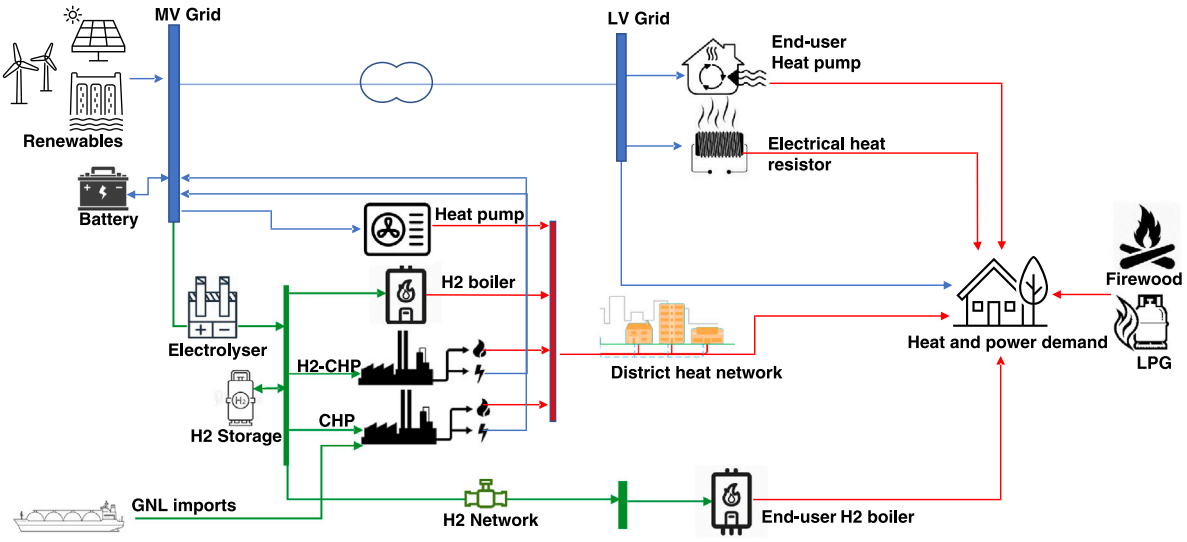

Fig. 1. Interaction between energy vectors.

next. Water reservoirs allow for water management within a day, but not across months, given their low storage capacity (which cannot be expanded due to environmental and social constraints in the case study area).

The model is formulated for an isolated system (remote areas far away from the large, national grid), considering the integrated planning across several energy vectors and networks—specifically electricity, heat, and hydrogen networks. The modelled region is disaggregated into a number of zones, which can be grouped into a number of microgrids, representing both the energy flows and respective networks between and within microgrids. The most important contribution of this work is incorporating the power flows using a full AC formulation, i.e. considering both active and reactive powers, in a multi-energy multi-microgrid system model. This is made possible by a convexification of the power flow equations that allows the model to be written in a mixed integer linear form.

Fig. 1 shows a diagram of the interactions between the energy vectors and technologies involved to satisfy heat and electricity service demands. As shown, heating demands can be supplied by a district heating network, by domestic hydrogen boilers connected to a hydrogen network, and by domestic air-source heat pumps or electric resistors connected to the electricity grid. In turn, the district heating network can be supplied by district-level air-source heat pumps, natural gas and hydrogen CHPs, and hydrogen boilers. These alternatives aim to fully or partially displace the use of firewood and liquefied petroleum gas currently used in the studied area, meeting annual CO_2 and particulate matter emission limits.

Electricity requirements are supplied by conventional generators, renewables and batteries. Hydrogen demand and storage is supplied by electrolysers. Thus, there are interactions between electricity–heat, hydrogen–heat and electricity–hydrogen energy vectors.

2.2. Model formulation

This section presents the main equations that describe the proposed model. The Nomenclature can be found in Appendix A, and the full model formulation is presented in Appendix B.

2.2.1. Objective function

The objective function, Eq. (1), seeks to minimise the annualised investment cost and the expected operating cost over one year. Each scenario is assigned with a probability of occurrence. It should be noted that the model considers existing infrastructure and technologies.

$$OF = \min \left\{ Inv + \sum_{s\in S} \sum_{t\in T} \rho_s Ope_{s,t} \right\} \tag{1}$$

The total investment costs (Eq. (2)) include investment in heat, electricity and hydrogen generation technologies, as well as storage in batteries and hydrogen tanks. As previously stated, investment costs for networks between zones and within zones are considered for each energy vector. For inter-zone grids, the decision variable corresponds to the link capacity (since the length is already known), while for intra-zone grids, the decision variable corresponds to the length (in kilometers) of the networks to be installed.

$$\begin{aligned} Inv = & \sum_{h\in H, n\in N} \pi_h^I \overline{H}_{h,n} + \sum_{g\in G, n\in N} \pi_g^I \overline{P}_{g,n} + \sum_{n\in N} \pi^{IBS} \overline{P}_n^{BS} \\ & + \sum_{n\in N} \pi^{IHS} \overline{P}_n^{HS} + \sum_{n\in N} \pi^{IP2G} \overline{P}_n^{P2G} + \sum_{n\in N} \pi^{kmDx} Km_n^{Dx} \\ & + \sum_{n\in N} \pi^{kmHN} Km_n^{HN} + \sum_{n\in N} \pi^{kmGN} Km_n^{GN} + \sum_{j\in \bar{J}} \pi^{IHN} D_j^{HN} \overline{F}_j^{heat} \\ & + \sum_{k\in \bar{K}} \pi^{IGN} D_k^{GN} \overline{F}_k^{gas} + \sum_{l\in \bar{L}} \pi_l^I \mu_l \end{aligned} \tag{2}$$

Operating costs, shown in Eq. (3), are composed of the variable costs of electrical generators; fuel consumption costs for firewood, liquefied petroleum gas, and natural gas; and non-supplied energy costs for both electrical and thermal energy.

$$\begin{aligned} Ope_{s,t} = & \sum_{n\in N, g\in G} \pi_g^O P_{g,n,s,t} + \sum_{n\in N} \pi^{LPG} C_{n,s,t}^{LPG} + \sum_{n\in N} \pi^{FW} C_{n,s,t}^{FW} \\ & + \sum_{n\in N} \pi^{LNG} G_{n,s,t}^{LNG} + \sum_{n\in N} \pi^{PLL} P_{n,s,t}^{LL} + \sum_{n\in N} \pi^{HLL} H_{n,s,t}^{LL} \\ & \forall s \in S, t \in T \end{aligned} \tag{3}$$

2.2.2. Energy balance equations

Eq. (4) represents the balance of the electricity vector. The net active power in each zone corresponds to the total demand, minus generation and non-supplied power. The total demand corresponds to the sum of current electricity demand and the potential electricity demands for heating and hydrogen production. The total active power generation is given by the sum of diesel generators, renewable generation, batteries

and co-generation. In turn, Eq. (5) indicates that the net reactive power in each zone is equal to the reactive demand in the zone, minus the reactive injection by generators and batteries.

$$P_{n,s,t} = P^{D}_{n,t} + \sum_{h\in\{Aux,HP,ASHP\}} P_{h,n,s,t} + P^{P2G}_{n,s,t} - P^{LL}_{n,s,t} - P^{BS}_{n,s,t} - \sum_{g\in G} P_{g,n,s,t}; \quad \forall n\in N, s\in S, \forall t\in T \tag{4}$$

$$Q_{n,s,t} = Q^{D}_{n,t} - Q^{BS}_{n,s,t} - \sum_{g\in G} Q_{g,n,s,t}; \qquad \forall n\in N, \forall s\in S, \forall t\in T \tag{5}$$

For the heat balance (Eq. (6)), heating demands can be supplied either by a district heating network, or by end-use technologies connected to distribution networks (in this case residential-size hydrogen boilers, air-source heat pumps, wood heaters, conventional electric heaters, and liquefied petroleum gas boilers). The district heating network can be supplied by natural gas CHPs, hydrogen CHPs, district level hydrogen boilers, and district-level air-source heat pumps.

$$H^{D}_{n,t} - H^{LL}_{n,s,t} = H^{dhn}_{n,s,t} + H^{endu}_{n,s,t}; \qquad \forall n\in N, \forall s\in S, \forall t\in T \tag{6}$$

Further equations for the district energy balance can be found in Appendix B.2, such as allowing bi-directional exchange of energy flows between two zones, and flows being constrained by network capacities.

For the hydrogen energy balance, it is considered that the sum of hydrogen produced by electrolysers together with the net power of hydrogen injected from storage, must equal the hydrogen consumed by district level and end-use boilers and CHPs, as shown in Eq. (7). Exchange of gas flows between zones is allowed, subject to the maximum capacity of pipelines to be installed (see Appendix B.2).

$$G^{P2G}_{n,s,t} + P^{HS}_{n,s,t} = \sum_{h\in\{CHP,EHB,HCHP,HB\}} G_{h,n,s,t} + \sum_{k\in From_n} f^{gas}_{k,s,t} - \sum_{k\in To_n} f^{gas}_{k,s,t}; \quad \forall n\in N, \forall s\in S, \forall t\in T \tag{7}$$

2.2.3. Power flows in low-voltage networks

The following formulation of AC power flows in the low-voltage networks connecting cities/zones and generation points is proposed, based on quadratic variables for voltage ($v_{n,s,t}$) in each zone, and current in each network line ($i_{m,n,s,t}$). See Appendix B.3 for the definition and bounds over voltages and currents. Eq. (8) relates the voltages between two consecutive zones, by the flows and losses of active and reactive power passing through the line that connects them, and its electrical parameters. This formulation was first introduced by [38].

$$v_{n,s,t} = v_{m,s,t} - 2(R_{m,n}P_{m,n,s,t} + X_{m,n}Q_{m,n,s,t}) + i_{m,n,s,t}(R^2_{m,n} + X^2_{m,n}); \quad \forall (m,n)\in N\times N, \forall s\in S, \forall t\in T \tag{8}$$

Eq. (9) defines the active power flow through the line connecting zones m and n as the net power at the arrival point of the line (n), a loss component proportional to the electrical resistance of the line, and the net flow coming into zone n from other points in the network. Similarly, Eq. (10) defines the reactive power flow in the line connecting two zones.

$$P_{m,n,s,t} = P_{n,s,t} + R_{m,n}i_{m,n,s,t} + \sum_{fr\ n=i} P_{i,j,s,t} - \sum_{to\ n=j} P_{i,j,s,t}; \quad \forall (m,n)\in N\times N, \forall s\in S, \forall t\in T \tag{9}$$

$$Q_{m,n,s,t} = Q_{n,s,t} + X_{m,n}i_{m,n,s,t} + B^{sh}_{n}v_{n,s,t} + \sum_{fr\ n=i} Q_{i,j,s,t} - \sum_{to\ n=j} Q_{i,j,s,t}; \quad \forall (m,n)\in N\times N, \forall s\in S, \forall t\in T \tag{10}$$

The above formulation is completed by the following non-linear equations. Eq. (11) models the apparent power capacity of the lines, while Eq. (12) relates the power flows to the voltage in the emitter zone and current in the line.

$$P^2_{m,n,s,t} + Q^2_{m,n,s,t} \le \overline{S}^2_{m,n}; \qquad \forall (m,n)\in N\times N, \forall s\in S, \forall t\in T \tag{11}$$

$$v_{n,s,t}\cdot i_{m,n,s,t} \ge P^2_{m,n,s,t} + Q^2_{m,n,s,t}; \qquad \forall (m,n)\in N\times N, \forall s\in S, \forall t\in T \tag{12}$$

In order to maintain tractability and a low computational solving time, the equations are further manipulated to become completely linear. Therefore, Eqs. (11) and (12) are approximated to linear Eqs. (13) and (14), respectively, by means of tangent lines and planes. While Eq. (13) was introduced by [39], Eq. (14) is introduced here for the first time by using the same principles.

$$-\frac{-\alpha P_{m,n,s,t} + \overline{S}_{m,n}}{\sqrt{1-\alpha^2}} \le Q_{m,n,s,t} \le \frac{-\alpha P_{m,n,s,t} + \overline{S}_{m,n}}{\sqrt{1-\alpha^2}}; \quad \forall (m,n)\in N\times N, \forall s\in S, \forall t\in T, \forall \alpha\in(-1,1) \tag{13}$$

$$\tilde{V}_n i_{m,n,s,t} \ge \tilde{P}^2_{m,n} + \tilde{Q}^2_{m,n} + 2\tilde{P}_{m,n}(P_{m,n,s,t} - \tilde{P}_{m,n}) + 2\tilde{Q}_{m,n}(Q_{m,n,s,t} - \tilde{Q}_{m,n}); \quad \forall (m,n)\in N\times N, \forall s\in S, \forall t\in T \tag{14}$$

Note that the region defined by the right-hand side of Eq. (14) corresponds to the linear approximation of the region defined by the right-hand side of Eq. (12) via supporting planes. This approximation is possible because Eq. (12) is convex if we assume that $\tilde{V}_n = 1[p.u.]$. Note also that $\tilde{P}_{m,n}$ and $\tilde{Q}_{m,n}$ can represent different predefined points that seek to discretise the $P-Q$ space (to simplify notation, Eq. (14) only presents a single supporting plane; still, more should be used to improve the resolution of the discretisation), over which the supporting planes or "cuts" are built (these "cuts" can be determined before we run the optimisation model or can be embedded within the optimisation model in a cutting plane algorithm to generate cuts more adjusted to the relevant operating points). $\tilde{P}_{m,n}$ and $\tilde{Q}_{m,n}$ should be selected such that:

$$\tilde{P}^2_{m,n} + \tilde{Q}^2_{m,n} \le \overline{S}^2_{m,n} \qquad \forall (m,n)\in N\times N \tag{15}$$

It is important to highlight that Eq. (14) is only useful to set a lower bound (right-hand side) for the current (or more specifically, its quadratic value) that is used to calculate the active and reactive losses (in Eqs. (8), (9), and (10)). So, only for the purpose to compute losses, we define voltages ($\tilde{V}_n$) equal to 1 [p.u]. For all other purposes, voltages ($v_{n,s,t}$) are determined by the model.

2.2.4. Energy distribution networks within zones

It is assumed that heat demand is evenly distributed over the roads within each zone. Under this assumption, each kilometre of network to be installed supplies a fraction of the city's peak thermal demand. This fraction is represented by the decision variable of kilometres of network to be installed for each network type, over the total road length in each zone in which demand is distributed.

In the case district heating networks, the sum of capacities of technologies connected to the network must be less than or equal to the fraction of the maximum demand of the area that will be supplied by this route [27], as seen in Eq. (16).

$$\sum_{h\in\{HP,CHP,HB,HCHP\}} \overline{H}_{h,n} \le Km^{HN}_{n}\frac{H^{max}_{n}}{Km_n}; \qquad \forall n\in N \tag{16}$$

The same principle is applied for the very low-voltage electricity network length, and for hydrogen networks lengths (see Appendix B.4). The very low-voltage network refers to the power distribution network within each zone.

2.2.5. Thermal power generation

Thermal power delivered by air-source heat pumps is equal to the electrical power consumed, multiplied by their Coefficient of Performance (COP), and is subject to their maximum capacity. The COP of these technologies varies depending on the outside temperature, decreasing their efficiency in colder days (see Appendix C). The thermal power delivered by hydrogen boilers is equal to the hydrogen consumed – in terms of its heating value – times the boilers' efficiency, and is also subject to their maximum capacity.

Two types of CHPs are also incorporated; a hybrid CHP fuelled by natural gas/hydrogen mixtures, and a CHP fuelled by pure hydrogen. Their thermal power production is bounded by their maximum thermal capacity and weighted by an availability factor which accounts for annual maintenance periods. In the case of hybrid CHPs, the hydrogen present in the mixture cannot exceed a maximum percentage in volume. Generation between one hour and the next cannot be greater than a maximum load shedding or load shedding ramp. See Appendix B.5 for details on all these constraints.

2.2.6. Hydrogen generation and storage

The hydrogen produced by the electrolyser is the active power consumed times a conversion efficiency. Its power consumption is limited to the electrical capacity of the electrolyser (see Appendix B.6).

Although the proposed model uses a typical day representation, it captures the capability of certain technologies to store energy seasonally. To do so, the model assumes that the state of charge of seasonal storage can gain (or lose) a net amount in a day, increasing (or decreasing) the state of charge (SOC) at the end of the day with respect to its value at the beginning of the day. As every day looks the same within a month (in one scenario), the model calculates the net increase (or decrease) in the SOC across the month by simply multiplying the daily gain in the SOC times the number of days in a month. This net increase (or decrease) in the SOC in a month is considered at the beginning of the next month. This is captured by the model in Eqs. (17)–(18) and Eqs. (B.43)–(B.45). The net charging power (discharge minus charging) is bounded by the storage tank's charging capacity, for the entire set of hours within each representative day. The energy contained in the tank cannot be greater than the maximum charging power multiplied by the duration of the storage in hours (Appendix B.6). Within each representative day and from the second hourly block onwards, the energy contained in a given hour is calculated as the energy contained in the previous hour, plus the load, and minus the discharge in the current hour, as shown in Eq. (17).

$$P^{HSE}_{n,s,t} = P^{HSE}_{n,s,t-1} - P^{HS-}_{n,s,t} + P^{HS+}_{n,s,t}\eta^{HS}; \quad \forall d \in D, \forall n \in N, \forall s \in S, \forall t \in \{24(d-1)+2, \dots, 24d\} \tag{17}$$

The initial condition $G^{HSE_0}_d$ for each representative day (except for the first), is calculated as a function of the initial condition and the state of charge in the 24th hour of the previous representative day, as shown in Eq. (18). See Appendix B.6 for border conditions.

$$G^{HSE_0}_{n,s,d} = (1-\eta^{loss}) \cdot (G^{HSE_0}_{n,s,d-1} + N^{days}_d \cdot (P^{HSE}_{n,s,t=24d} - G^{HSE_0}_{n,s,d-1})); \quad \forall d \in D, \forall n \in N, \forall s \in S \tag{18}$$

2.2.7. Electricity generation and storage

Eq. (19) models plants with regulation capacity and corresponds to a known end-point model. Here, the sum of the active powers in a set of hours T_m cannot exceed generation capacity of the reservoir weighted by a load factor, and weighted by the cardinality of the set. This model is used for small and medium-sized reservoirs over short time horizons, deciding the movement of energy within a period (e.g., one day), but not between periods. Given the social constraints in the case study system, large capacity reservoirs are not considered.

$$\sum_{t \in T_d} P_{g,n,s,t} \le \overline{P}_{g,n} PF^{Dam}_{n,s,d} Card(T_m); \quad \forall d \in D, \forall g \in \{Dam\}, \forall n \in N, \forall s \in S \tag{19}$$

For non-dispatchable renewable power plants, power generated in each hour cannot exceed the plants' capacities times the resource availability in that hour. For diesel power plants, generated power is capped by their capacity. Additionally, the power difference between two consecutive hours must not exceed the maximum load shedding ramp. See Appendix B.7 for further details.

The operating chart relating active and reactive power of each generator with its capacity is modelled according to Eq. (20). As for transmission limits on the lines, tangent lines which form the feasible region of the active and reactive power operating points are defined. Under the assumption that wind and solar generators will seek to inject maximum active power – because more sophisticated control strategies are required for reactive power injection – it was imposed that only synchronous generators can inject reactive power (i.e. diesel generators, run-of-river and reservoir hydroelectric generators).

$$-\frac{-\alpha P_{g,n,s,t} + \overline{S}_{g,n}}{\sqrt{1-\alpha^2}} \le Q_{g,n,s,t} \le \frac{-\alpha P^g_{n,s,t} + \overline{S}_{g,n}}{\sqrt{1-\alpha^2}} \quad \forall \alpha \in (-1,1), \forall g \in G, \forall n \in N, \forall s \in S, \forall t \in T \tag{20}$$

For batteries, a predetermined duration model is used, in which the investment decision variable is the battery's charging capacity or power. This is, the model decides the power for a set of possible durations. Charging and discharging power must be less than the battery's capacity. In addition, the energy stored in the battery must not exceed its capacity multiplied by the charging duration. Charge states are coupled using an inventory constraint, and the reactive power that can be injected by the battery is modelled in the same way as for generators (see Appendix B.7).

2.2.8. Following heat demand profile

A set of constraints are included for end-use heat technologies so that they cannot only operate on peak demands, reflecting that each customer does not have access to a pool of heat supply technologies (i.e. each customer has one type of heat supply technology in their homes). See details for all of these constraints in Appendix B.8. The sum of heat outputs generated by the technologies connected to the district heating network must follow the heat demand profile. The same applies for end-user hydrogen boilers, and for the sum of outputs of residential heat pumps with auxiliary electric heaters. The profile to be followed by these three technology groups (district heat, hydrogen boilers, and heat-pump/auxiliary electric heater units) can be either the total heat demand profile, the domestic hot water profile, or the space-heating demand profile.

For the cases of firewood and LPG technologies, firewood must follow space-heating demand profiles and LPG must follow water-heating demand profiles, as the current associated technologies supply these energy service demands specifically, and there is no replacement between them. On the other hand, we impose that firewood and LPG consumption cannot be higher than the current use.

2.2.9. Emission limits

Finally, in order to study cost-effective decarbonisation and decontamination pathways in the case study region, we include emission limits consistent with Chile's NDCs. Eq. (21) caps the expected annual sum of CO_2 emissions due to the use of diesel, natural gas and liquefied petroleum gas, while Eq. (22) limits the expected particulate matter produced by the use of firewood. It is worth noting that although firewood produces CO_2 in its combustion, in this work it is considered carbon neutral (as indicated by the Chilean energy policy) and is therefore not considered in Eq. (21).

$$\sum_{s \in S} \sum_{n \in N} \sum_{t \in T} \rho_s (P_{g=Oil,n,s,t} CE_{oil} + G^{LNG}_{n,s,t} CE_{LNG} + C^{LPG}_{n,s,t} CE_{LPG}) \le CET \tag{21}$$

$$\sum_{s \in S} \sum_{n \in N} \sum_{t \in T} \rho_s C^{FW}_{n,s,t} PM^{FW} \le PMT \tag{22}$$

Table 1
Plant type and generation capacity.

Plant name	Type	Capacity [MW]
Puerto Aysén	Run-of-river hydroelectric	6.8
Monreal	Run-of-river hydroelectric	3
Lago Atravesado	Hydroelectric with regulation capacity	11
Alto Baguales	Wind power plant	3.78
Aggregated diesel[a]	Diesel power plants	32.3
San Víctor	Run-of-river hydroelectric	3

[a]4 diesel power plants located in the towns of Puerto Chacabuco, Puerto Aysén, Coyhaique, Villa Mañihuales and Puerto Ibáñez.

3. Case study and input data

The described model is applied to a real network located in the south of Chile: the Aysén Medium-sized System (SMA). This is one of the three electricity systems present in the Aysén Region, which is isolated from the Chilean National Electricity System. The Aysén Region is located in the southern part of Chile, in Patagonia, has a population of around 105000 inhabitants, and a surface area of around 108 [km^2]. It has a cold oceanic climate with low temperatures, abundant rainfall, strong winds and high humidity, with an annual average temperature of approximately 8 °C.

Although 80% of its annual electricity generation comes from hydroelectric and wind energy [40], the intensive use of firewood for heating has led it to become one of the most polluted systems in the continent. Firewood has a penetration of 98.2% for space-heating demands in the residential sector, and is responsible for 87% of fine particulate matter emissions in this sector [41]. The SMA's pollution problem is so severe that a 2018 study by the World Health Organisation (WHO) ranked the city of Coyhaique, the capital of this region, as the most polluted city in the Americas [42]. Additionally, the system relies mostly on LPG for domestic hot water supply, producing high levels of CO_2 emissions.

On the other hand, the geographical area of this system stands out for its high potential of renewable resources, which are arguably sufficient to supply heat and electricity demands in a sustainable way, reducing firewood consumption – and thus pollution – without the need of fossil fuels. Although the option of electrifying heat is straightforward, alternatives such as district heating, CHPs, and hydrogen technologies for heating, among others, could be potentially competitive and could reduce the extra electricity infrastructure required to supply high levels of heat demands, when planned in an integrated optimum way.

3.1. Existing system

Input data includes the capacity of existing infrastructure which is considered as a sunk cost, for both heat and electricity generation technologies. Currently, the case study system only has an electricity grid, i.e. it has no district heating networks, gas networks, hydrogen networks, nor LNG regasification terminals. The main fuels used for electricity generation in the region are diesel and LPG. Additionally, firewood is the main fuel used for space-heating, while LPG is the main fuel used for domestic hot water supply. Table 1 shows the system's generation capacity and plant type.

The topology of the electricity system is radial, with long low-voltage lines between the main generation and demand points of the system. Therefore, the voltage profiles and the presence of reactive power is not negligible, which makes the convex power flow model necessary.

3.2. Candidate networks and technologies

Fig. 2 shows the single phase diagram which includes both, the existing infrastructure, and the candidate technologies and networks that the model can choose to install, for the complete system.

Table 2 shows the candidate technologies that the model can choose to install for each microgrid shown in Fig. 2. Each microgrid groups several zones (that are presented as nodes in Fig. 2). Each zone corresponds to a small town, except for Alto Baguales, Lago Atravesado and Monreal that are generation-only nodes. In this context, each group of zones is treated as a microgrid, which can operate isolated from the rest of the system, if needed, as every microgrid is equipped with generation with the ability to control frequency.

Finally, interconnection between the three microgrids is only considered through reinforcing the existing power lines by means of parallel lines (i.e. reinforcement line between Puerto Aysén-Alto Baguales, and between Alto Baguales-Villa Ortega). This assumption is due to the long distances between microgrids that would make district heating networks non-viable, added to low thermal demands which make gas/hydrogen pipelines not competitive against electricity lines.

3.3. Estimation of energy service demands

The electricity demand profile for each representative day is presented Appendix D, Fig. 17. The profiles were obtained based on a National Energy Commission's study [40] and correspond to projected profiles for the year 2020 (simulation year). Profiles were published with an hourly resolution, and representative days were obtained as average days of each month.

Heat demand profiles for each representative day are presented in Appendix D, Fig. 18, which represent the sum of space-heating and hot water demand profiles. Annual domestic hot water demand was estimated using regional LPG demand in the residential sector [4] – assuming an LPG boiler combustion efficiency – weighted by the proportion of customers supplied by the SMA out of the region's total customers. According to [43], 58% of LPG demand is for domestic hot water use, discounting consumption for cooking and others. Normalised annual hourly profiles were taken from [44], and daily averages for each month were used as representative days. Heat demand was allocated into zones proportionally to electricity demand.

Space-heating in the region is currently supplied by firewood. Annual regional heat from firewood [41] was weighted by the fraction of customers in the region that are supplied by the SMA system. For hourly profiles, a factor H proportional to the difference between outside temperature and a comfort temperature of 18 ° C in each hour of the year was adjusted (Eq. (23)).

$$H_t^{Fwood} = H \cdot (Tamb_t - 18°) \tag{23}$$

Where H_t^{Fwood} is heat supplied by firewood in hour t, $Tamb_t$ is the outside temperature in hour t, and factor H is such that the sum of firewood heat demand over all hours of the year is equal to the annual firewood heat demand. Hourly temperatures for a full year were obtained from historical meteorological data for the region, using verified data of the year 2018 [45].

Table 3 shows the distribution of total annual heat and electricity demands of the system per zone. Linear heat density represents annual heat demand divided by the total road length over which demand is distributed [28].

3.4. Renewable generation profiles

Hourly profiles for run-of-river hydropower generation and monthly load factors for regulated hydropower plants were obtained from [40]. This reference contains annual hourly generation profiles for each existing hydro power plant between 1990 and 2016. Based on this data, three hydro profile scenarios were obtained for each plant, representing

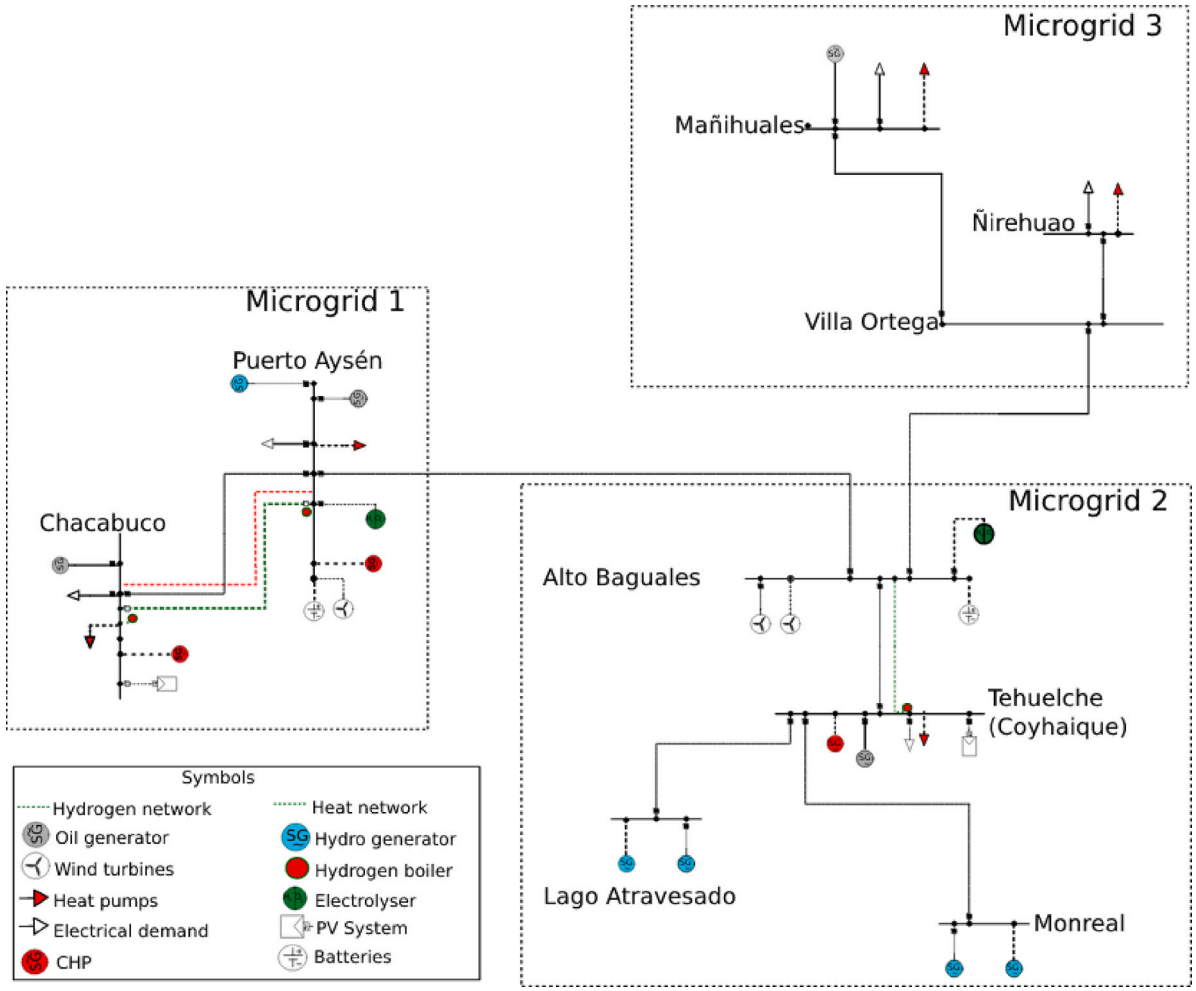

Fig. 2. System's unilinear diagram with existing and candidate technologies and infrastructure per microgrid and zone.

a dry, average, and wet scenario. Based on the number of years that each scenario represents over the total number of years, the probability of occurrence of each hydro scenario was determined, resulting in 60%, 30% and 10% for the wet (H1), medium (H2) and dry (H3) scenarios, respectively.

Profiles for solar and wind generation were obtained from [46,47], respectively. For wind generation, profiles were extracted based on historical annual hourly data for the period between 1980–2013. Three profile scenarios were constructed with the historical data, taking the highest, average, and lowest load factors of the sample. The probability of occurrence of each scenario was determined by clustering the historical data using the three aforementioned profiles as references (or centroids). The resulting probabilities were 1/34, 30/34 and 3/34 for the scenarios of high (W1), medium (W2) and low (W3) wind resource availability, respectively. In the case of solar power, due to its higher certainty levels, we use a single profile scenario built based on historical data.

The 3 hydrological scenarios were combined with the 3 wind availability scenarios to form a total of 9 scenarios, shown in Fig. 3. The figure shows the probability of occurrence of these 9 scenarios, obtained from multiplying the probability of the wind and hydrological scenarios that comprise them.

To sum up, our quantifications capture 12 representative or typical days with an hourly resolution for demand, each one representing the characteristics of a month of the year (one day per month). Each of these days features 9 possible hourly profiles of available renewable resources, each one representing the characteristics of a month of the year. Hence, the model can capture hourly fluctuations of demand and renewable resources across a day, seasonal patterns of demand and renewables through the representation of different months, and the uncertainty associated with the availability of wind and hydro resources. Overall, the model considers 108 possible realisations of a day with an hourly resolution, leading to 2592 operating conditions (each daily profile of demand and renewable resources features 24 h). Although the number of operating conditions can be increased and the model is sufficiently flexible to do that, this number of operating conditions is sufficient for long-term investment planning (including generation and network assets) and policy purposes and aligned with similar studies such as [48]. Furthermore, we recognise that increasing the problem's size may require more advanced algorithms, but this paper does not aim to contribute at this level.

Regarding the probabilities, each of the 12 days weighs 1/12, and the probability of each of the 9 combined wind/hydro scenarios is calculated assuming that wind and hydro profiles are independent and by associating historical data (daily profiles) to one of the chosen representative scenarios, counting the frequency of occurrence of each representative daily profile.

3.5. Costs of technologies

Table 4 presents investment and variable costs for electricity generation technologies [49] used in this study. For the case of batteries, a cost per energy capacity of 550 [USD/MWh] was assumed to calculate capacity costs for 2- and 4-hour batteries.

Table 2
Candidate networks and technologies per microgrid and zone.

Microgrid 1
• Wind power plant in Puerto Aysén + batteries • Solar generation in Chacabuco zone • Natural gas CHP • Hydrogen CHP • District heating network within each zone • End-use air-source heat pumps and conventional electric heaters in each zone + reinforcement of the very low voltage network • Electrolyser and hydrogen storage in Puerto Aysén • Hydrogen distribution network + end-use boilers in each zone • Hydrogen network between both zones • Heat network between both zones • Electricity line reinforcement between both zones (parallel lines)
Microgrid 2
• Wind power plant in Alto Baguales + batteries • Run-of-river hydroelectric plant in Monreal • Reservoir hydroelectric power plant in Lago Atravesado • Solar PV plant in Coyhaique • Hydrogen network between Alto Baguales and Coyhaique • Hydrogen distribution network + end-use boilers in Coyhaique • Natural gas CHP • Hydrogen CHP • District heating network in Coyhaique • End-use air-source heat pumps and conventional electric heaters in Coyhaique + reinforcement of the very low voltage network • Electricity line reinforcement between zones (parallel lines)
Microgrid 3
• Villa Ortega zone is considered as an intermediate zone with no demand nor generation • End-use air-source heat pumps and conventional electric heaters + reinforcement of the very low voltage network within the two other zones • Electricity line reinforcement between zones (parallel lines)

Table 3
Distribution of total demand per zone and linear heat density.

Zone	Annual electricity demand [MWh]	Annual heat demand [MWh]	Network length [km]	Linear heat density [MWh/km]
Chacabuco	21.576	107.520	30	3.584
Puerto Aysén	24.997	124.492	60	2.075
Tehuelche	86.697	431.781	90	4.798
Mañihuales	2.374	11.932	15	795
Ñirehuao	347	1.730	6	288
Total	135.991	677.456	201	3.370

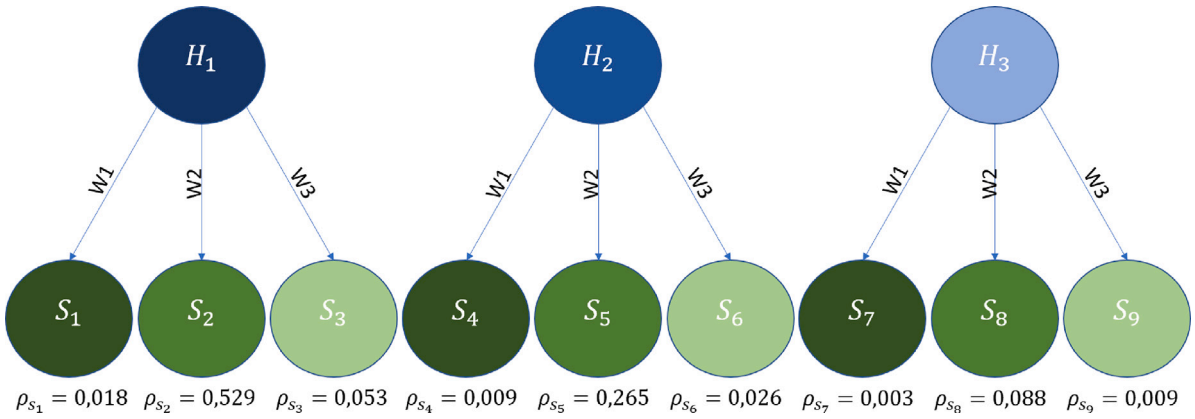

Fig. 3. Scenario probability of occurrence.

Techno-economic parameters for inter-zone and intra-zone networks are presented in Table 5, and techno-economic parameters used for heat and hydrogen technologies are shown in Table 6.

The annuities of these investments were calculated for each technology according to Eq. (24), where c_i represents the annualised investment cost of technology i, t represents its lifetime, r is the discount rate considered as 10%, and C_i is the total investment cost.

$$C_i = c_i \cdot \frac{1}{r}\left(1 - \frac{1}{(1+r)^t}\right) \tag{24}$$

Finally, Table 7 shows the costs, heating values, and emission factors for the fuels used in this work.

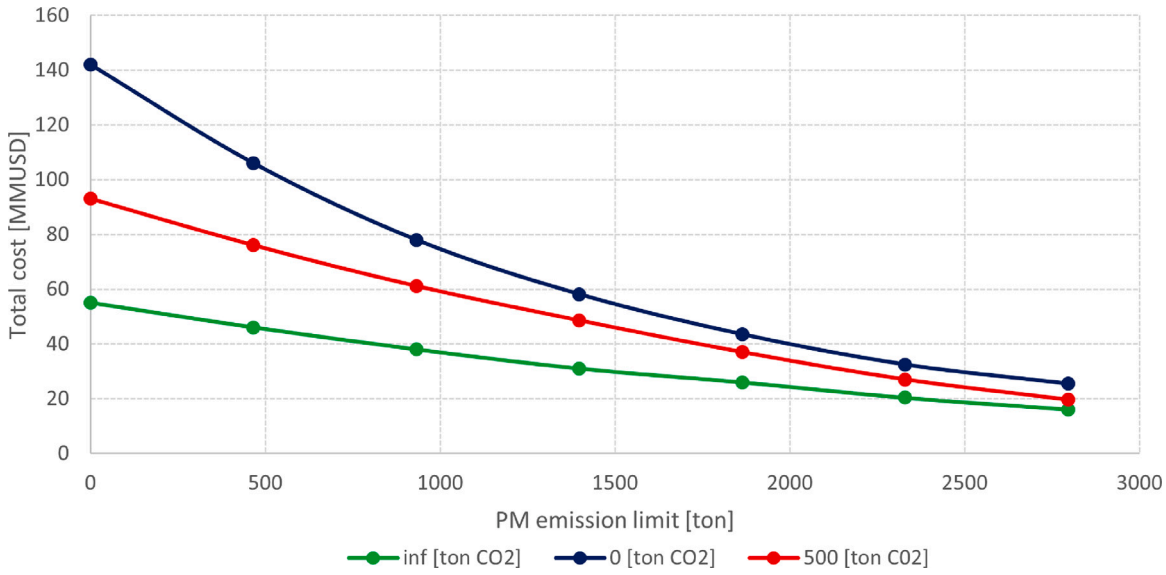

Fig. 4. Total system's cost for different particulate matter limits.

Table 4
Electricity generation technology costs [49].

Technology	Investment cost [USD/kW]	Variable cost [USD/MWh]	Lifetime [years]
Wind	1900	–	25
Solar	1000	–	25
Hydro run-of-river	3000	0.1	40
Hydro reservoir	3200	–	40
Batteries @2 h	1100	–	15
Batteries@4 h	2200	–	15
Diesel	500	120	20

Table 5
Techno-economic parameters for networks between and within zones [22,23,50].

Network	Between zones [USD/km*KW]	Within zones [USD/km]	Lifetime [years]
Electricity	3.10	62000	40
Hydrogen	4.06	154000	50
Heat	7.77	768000	50

3.6. Case studies

The following cases were defined to study the impact of different decarbonisation and decontamination pathways over total system costs and optimal technology mixes:

- **Case 0**: Firewood and LPG consumption are set as equal to the current consumption. This scenario is equivalent to planning only the electricity energy vector, restricted to not investing in new diesel power plants but only in renewables and batteries, together with grid expansion. This case yields the expected emissions of particulate matter and direct CO_2 for the base or current case.
- **Case 1**: There are no constraints over expected particulate matter and direct CO_2 emissions. Firewood and LPG use is also unconstrained, unlike Case 0. The relevance of this case is that it allows to know if the current solution can be optimised when carrying out an integrated planning.
- **Case 2**: A zero limit on direct CO_2 emissions is set, while particulate matter is unconstrained. This case indicates the cost of displacing LPG and current diesel generation with a 100% renewable electricity system.
- **Case 3**: Particulate matter and direct CO_2 emissions are limited to one-sixth and half of those resulting from Case 0, respectively. Particulate matter limits represent, in a simplified manner, a reduction of these emissions to levels recommended by the WHO. Direct CO_2 emissions reductions seek to avoid the intensive use of existing diesel for electricity generation.
- **Case 4**: Particulate matter emissions are limited to zero, while direct CO_2 emissions are unrestricted. This case reveals the cost of full replacement of firewood.
- **Case 5**: A zero limit is imposed on both particulate matter and direct CO_2 emissions. This case represents a 100% renewable and direct emission-free system.

The proposed model was implemented in FICO®Xpress Optimisation [53] and solved using Newton's numerical barrier method.

4. Results and discussion

4.1. Cost curves versus emission limits

Fig. 4 presents the total system costs which correspond to the value of the objective function for different particulate matter emission limits, for three levels of direct CO_2 emission limits. Fig. 5 presents these same curves normalised to the total system demand (sum of heat plus electricity demand), in order to obtain a price signal for each MWh supplied in each scenario. As expected, costs increase significantly when requiring lower particulate matter emissions, with a drastic increase for levels below 1000 [ton]. Additionally, it is clear that lowering CO_2 emission levels increases the system's cost, since diesel-fuelled power generation infrastructure must be replaced.

Similarly, Fig. 6 shows the total systems' costs against different direct CO_2 emission limits, for three different levels of particulate matter emissions. Fig. 7 presents the unit costs per MWh supplied for these cases. Costs are seen to increase significantly when restricting the expected CO_2 emissions. By forcing direct CO_2 emissions to zero, costs are considerably higher than for a limit of 2000 [ton]. This is because under a zero direct emissions constraint, existing diesel generators cannot operate, including the most extreme scenarios in terms of unavailability of renewable resources. The increase is even more drastic when imposing lower emission limits for particulate matter, as higher investments in electricity infrastructure are required to supply the new electricity demand that arises from heating when firewood is replaced.

Table 6
Techno-economic parameters for heat and hydrogen technologies [22].

Technology	Investment cost [USD/kW]	Efficiency (or COP)	Lifetime [years]
CHP	1050	0.6 electric 0.3 thermal	30
District air-source heat pumps (ASHP)	680	2–4	20
End-use ASHP	1037	2–4	20
Electric resistance heater	245	0.9	15
Electrolyser	1000	0.65	20
Hydrogen storage	1900	0.9	30
District hydrogen boiler	105	0.9	20
End-use hydrogen boiler	97	0.9	20

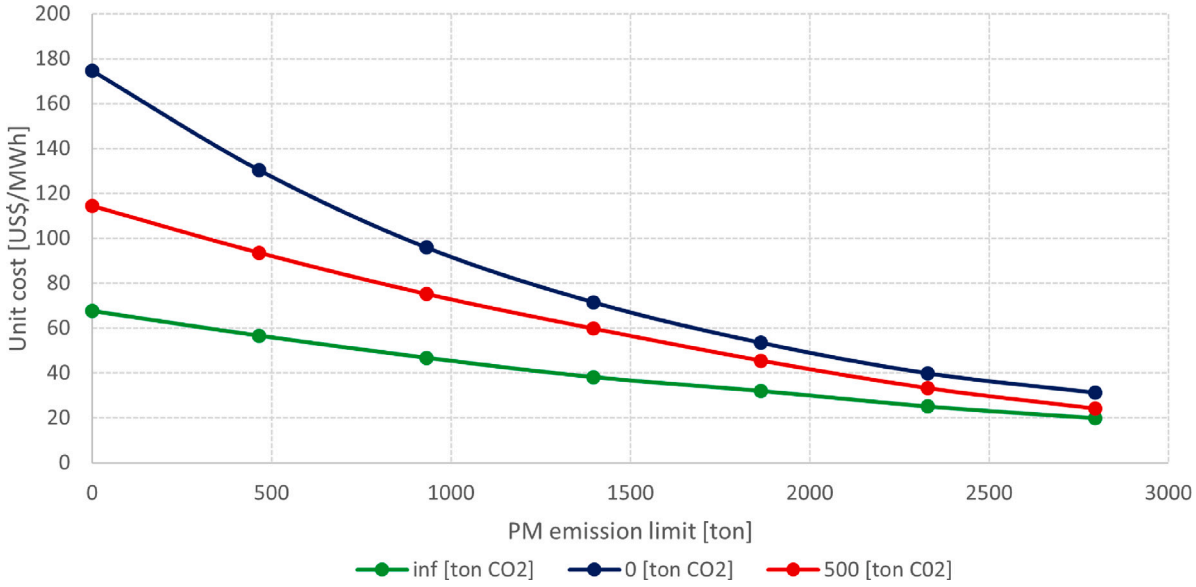

Fig. 5. Unitary cost for different particulate matter limits.

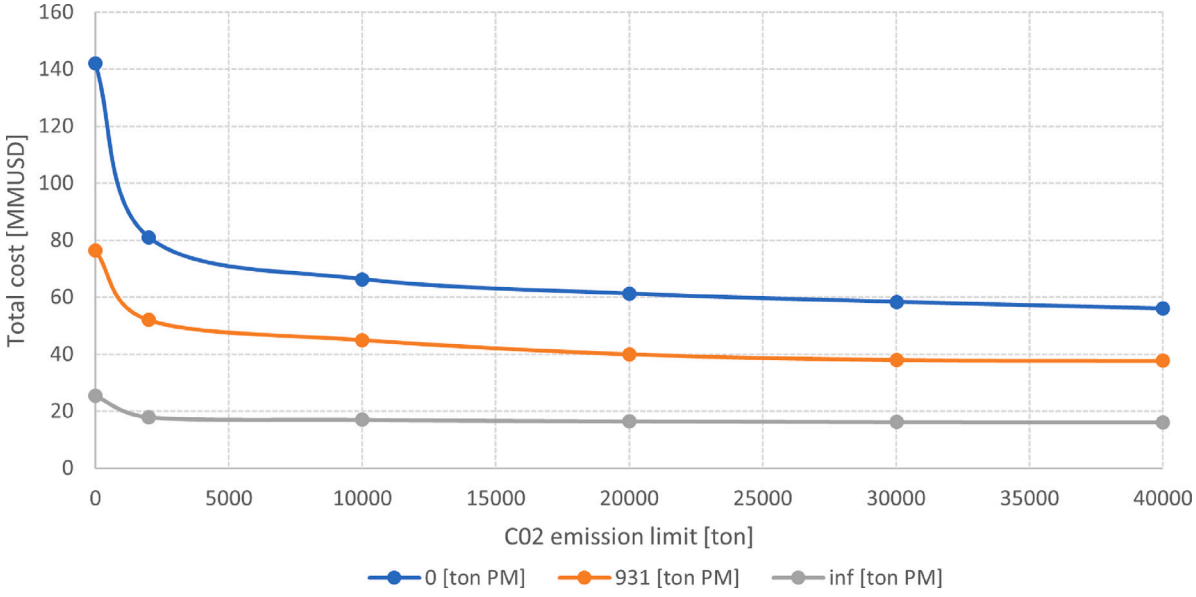

Fig. 6. Total system's cost for different direct CO_2 emission limits.

4.2. Energy portfolios and metrics

Table 8 shows the optimal portfolios for the six cases, together with their total systems' costs, operating costs, investment costs, and unitary costs (costs divided by the sum of heat and electricity demand). In the last row of this table, the unitary cost calculation is repeated, but adding the valuation of currently installed infrastructure. This allows to estimate the impacts of the imposed restrictions over tariffs for final customers. Table 9 also includes investment costs in networks between and within zones.

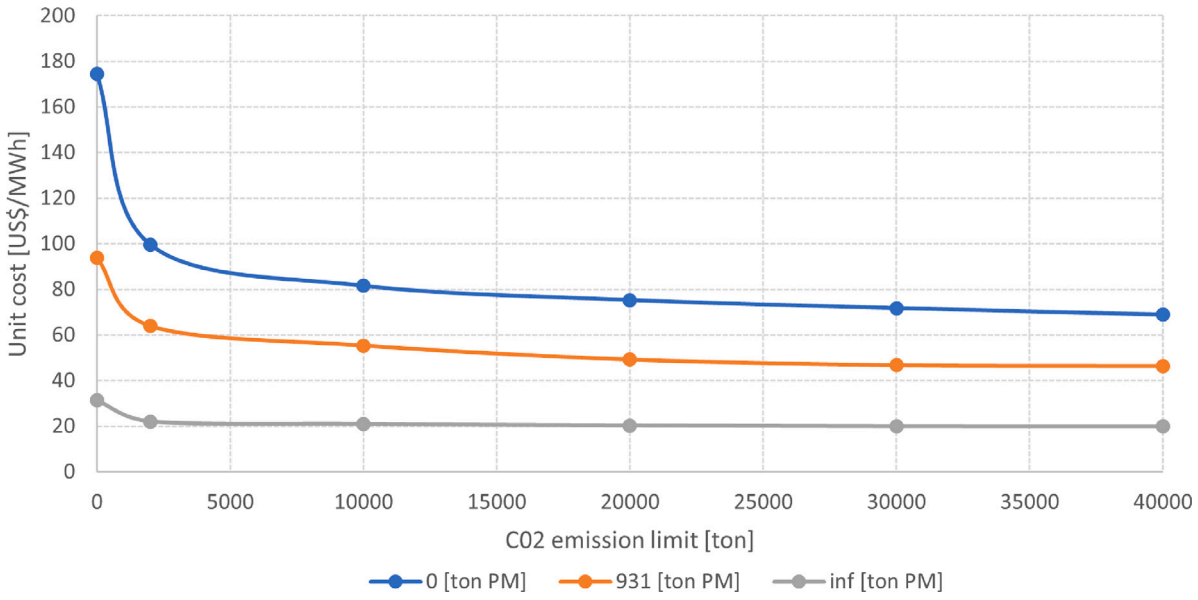

Fig. 7. Energy unit cost for different direct CO_2 emission limits.

Table 7
Fuel costs and emission factors [40,49,51,52].

Fuel	Cost	Higher heating value	Emission factor
Firewood	24 [USD/m^3]	1.28 [MWh/m^3]	5.98 [kgMP/m^3]
LPG	1.25 [USD/kg]	0.0146 [MWh/kg]	3.1 [kgCO2/kg]
Diesel	120 [USD/MWh]	–	0.84 [tonCO2/MWh]
LNG	80 [USD/MWh]	–	0.4 [tonCO2/MWh]

In **Case 0** there are no investments as a result of the optimisation. Es expected, since there is no demand growth compared to the base year in the assessment horizon, the model chooses to operate the system with the existing electricity infrastructure, and with firewood and LPG for supplying space-heating and domestic hot water, respectively. In **Case 1**, by allowing the optimisation of the heating sector, the model shifts considerably from LPG – and slightly from firewood – to using end-use ASHP along with electric heaters, and increasing 2.9 [MW] of wind generation capacity. This results in the total system's cost being reduced by 15%, in a reduction of 39% in direct CO_2 emissions, and of 0.5% in particulate matter, despite there being no limits on emissions. Investments are made in electricity networks within zones, but not between zones.

The comparison between **Cases 0** and **1** show that the current situation can be optimised in terms of economic and environmental performance, validating the hypothesis of the benefits of integrated planning. On the other hand, it can be inferred that firewood does not tend to be displaced by price signals, given its low operating cost (24 [US $/m^3]) and high heating value (1.28 [MWh/m^3]).

In **Case 2**, total costs increase by 34% compared to **Case 0**. Imposing a zero limit on direct CO_2 emissions results in a 1.3% reduction in particulate matter emissions. Since diesel generators cannot operate, the model invests in wind, hydro dam and run-of-river, solar, and battery generation technologies. Despite having low plant factors in this region, investment in solar generation is justified by the fact that it does not require installing additional lines between zones, or from the point of generation to the point of consumption. End-use ASHPs together with electric heaters continue to replace LPG as a heating fuel as for **Case 1**, with a slight increase (4.4 [MWth], 26%) in ASHP investments and a slight reduction (4.2 [MWth], 57%) in investment in conventional heaters compared to **Case 1**. Since firewood is very economical compared to investment costs in other technologies and because it is considered carbon neutral, it is not naturally displaced without restrictions on particulate matter emissions.

Case 3 shows a total cost increase of 180%, and a reduction of approximately 83% and 50% in particulate matter and direct CO_2 emissions respectively, compared to **Case 0**. As in **Cases 1** and **2**, the model decides to invest in ASHPs and electric heaters in order to displace LPG for domestic hot water. In this case, they also displace firewood for space-heating, given the emission limits imposed. Results show investments in wind and hydro generation, and in batteries, but as opposed to **Case 2**, there is no investment in solar generation. In this case investments are made in power lines between zones, reinforcing the Baguales-Tehuelche, Tehuelche-Lago Atravesado and Tehuelche-Monreal lines with parallel lines. This is because greater capacity is required to transmit electricity from zones where there is wind and hydroelectric generation, to demand zones, which increased because of a higher peentration in ASHPs.

For **Case 4**, there is an increase of 189% in total costs compared to **Case 0**. Total firewood displacement imposed by the zero particulate matter constraint, leads to an increase of 300% of direct CO_2 emissions compared to **Case 0**. Here, the model decides to invest in CHPs and district level ASHPs, requiring infrastructure for district heating networks within the zones of Puerto Chacabuco and Coyhaique. The only line reinforcement required in this case is the one connecting Tehuelche and Lago Atravesado. Investments in run-of-river hydro, wind generation, and batteries decrease with respect to **Case 3**, as CHPs also contribute to electric capacity. Additionally, a greater use of existing diesel generation is observed. Investments in district heating networks are triggered by the CO_2 emissions relaxation, as it is more cost-effective for the model to invest in CHPs fuelled by imported natural gas and co-generate heat and electricity, than to invest in ASHPs, reinforcement of low and very low voltage power lines (lines between zones and within zones), and new renewable power plants. On the other hand, comparing **Cases 2** and **4** shows that displacing wood for space-heating is significantly more expensive than displacing LPG for domestic hot water.

Finally, **Case 5** shows an increase of 650% in total costs compared to **Case 0**. This is the only case in which the model decides to invest in electrolysers and hydrogen-fuelled CHPs, although end-use ASHPs still predominate. Because this is a zero-direct-emission system, both short-term storage in batteries and seasonal storage using hydrogen become necessary. Unlike hydrogen, batteries cannot store energy from month to month, limiting the flexibility to shift surplus electricity from months

Table 8
Technology mixes and costs for the 6 cases.

	Case 0	Case 1	Case 2	Case 3	Case 4	Case 5
Total cost [MM USD]	18.99	16.12	25.48	53.44	54.96	142.42
Investment cost [MM USD]	0.00	3.02	14.41	49.98	40.21	142.41
Operation cost [MM USD]	18.99	13.10	11.07	3.46	14.75	0.01
Direct CO_2 emissions [ton]	22087	13488	0	11043	88338	0
PM emissions [ton]	2796	2781	2759	466	0	0
Non-supplied energy (electric)	0	0	0	0	0	0
Non-supplied energy (thermal)	0	0	0	0	0	0
CHP [MWth]	0	0	0	0	22.3	0
CHP-H2 [MWth]	0	0	0	0	0	6.9
District ASHP [MWe]	0	0	0	0	11.6	9.66
District ASHP [MWth]	0	0	0	0	29.71	24.74
End-use ASHP [MWe]	0	6.6	8.3	63.9	55.3	65.8
End-use ASHP [MWth]	0	16.9	21.3	163.6	141.6	168.5
District boilers [MWth]	0	0	0	0	0	0
End-use boilers [MWth]	0	0	0	0	0	0
Electric resistance heater [MWth]	0	7.3	3.1	6.2	1.9	0.0
Electrolyser [MWe]	0	0	0	0	0	15.2
Hydro dam [MW]	0	0	5.9	18.5	21.2	34.5
Hydro run-of river [MW]	0	0	10.2	41.1	13.4	95.8
Wind [MW]	0	2.9	19.9	47.1	1.34	328.7
Solar [MW]	0	0	18.7	0	0	5.8
Battery [MW]	0	0	4.3	7.3	5.8	13.1
Total unitary cost [USD/MWh]	23.35	19.82	31.32	65.70	67.56	175.08
Investment unitary cost [USD/MWh]	0.00	3.71	17.71	61.44	49.43	175.07
Operation unitary cost [USD/MWh]	23.35	16.08	13.61	4.25	18.13	0.01
Tariff cost final customer [USD/MWh]	39.40	35.87	47.37	81.75	83.61	191.13

Table 9
Investments in networks for the 6 cases.

Networks between zones (electricity/heat/hydrogen) : 1 if installed, 0 if not						
Line	Case 0	Case 1	Case 2	Case 3	Case 4	Case 5
Chacabuco-Pto Aysén	0/0/0	0/0/0	0/0/0	0/0/0	0/0/0	0/0/1
Pto Aysén-Baguales	0/0/0	0/0/0	0/0/0	0/0/0	0/0/0	0/0/0
Baguales-Tehuelche	0/0/0	0/0/0	0/0/0	1/0/0	0/0/0	1/0/0
Tehuelche-L.Atravesado	0/0/0	0/0/0	0/0/0	1/0/0	1/0/0	1/0/0
Tehuelche-Monreal	0/0/0	0/0/0	0/0/0	1/0/0	0/0/0	1/0/0
Alto Baguales-Villa Ortega	0/0/0	0/0/0	0/0/0	0/0/0	0/0/0	0/0/0
Villa Ortega-Mañihuales	0/0/0	0/0/0	0/0/0	0/0/0	0/0/0	0/0/0
Villa Ortega-Ñirehuao	0/0/0	0/0/0	0/0/0	0/0/0	0/0/0	0/0/0
Networks within zones (electricity/heat/hydrogen): installed km						
Chacabuco	0/0/0	3.67/0/0	3.67/0/0	23.26/0/0	16.87/11.79/0	1.15/28.75/0
Puerto Aysén	0/0/0	7.34/0/0	7.34/0/0	30.98/0/0	53.07/0/0	60/0/0
Tehuelche	0/0/0	11.02/0/0	11.02/0/0	89.34/0/0	63.45/26.17/0	90/0/0
Mañihuales	0/0/0	1.83/0/0	1.83/0/0	1.83/0/0	14.60/0/0	15/0/0
Ñirehuao	0/0/0	0.73/0/0	0.73/0/0	0.73/0/0	5.34/0/0	6/0/0

with higher resources and lower demands to months with higher heat requirements. For inter-zone networks, the same investments as in **Case 3** are required, plus the construction of a hydrogen network between Puerto Aysén and Puerto Chacabuco. Also, a district heating network is built in Puerto Chacabuco. All zones require reinforcement of their distribution networks due to heat electrification.

4.3. System operation

This section describes the expected annual operation for **Case 0** (baseline) and **Case 3** (PM emissions under WHO's limit). Fig. 8 shows the expected thermal operation for each representative day in **Case 0**, which represents the current operation of firewood and LPG technologies. Fig. 9 shows the expected operation of electricity generation technologies. Power generation is mostly based on renewable sources, with existing diesel generation operating in months in which there is a lower load factor for hydro dam power plants. Wind generation is observed to be higher in the summer months.

Figs. 10 and 11 show the operation of July's representative day (the day in the year with the highest demand) in the scenario of lower availability of renewable resources for thermal and electricity system, respectively. For thermal operation shown in Fig. 10, peak demand occurs around 8 am in the morning with the highest domestic hot water consumption. Electricity demand on this day is mainly supplied by hydroelectric generation, since the wind generation profile is low. The hydro dam power plant modulates diesel operation in order to optimise the system operation. Since there is no electrification of heat, the electricity generation profile has no relation to the thermal demand profile.

Fig. 12 shows the expected thermal power operation in each representative day for **Case 3**. Throughout the year, heat demand is supplied mainly by ASHPs, which supply both domestic hot water and space-heating requirements. The use of firewood decreases considerably compared to **Case 0**, maintaining it's hourly profile throughout the year, but in a smaller proportion. This means that some households continue to use firewood for space-heating while replacing LPG with ASHPs to supply domestic hot water demands. The rest of the dwellings supply their total heat demands using ASHPs. Conventional electric resistor heaters only operate during the hours when ASHPs decrease their COPs due to the lower ambient temperature.

Fig. 13 shows the expected electric power operation. In contrast to **Case 0**, because of heat electrification via ASHPs, the generation profile follows the heat load profile. Given higher investments in renewables driven by emission targets, wind generation takes on a higher relevance compared to **Case 0**, with diesel generation operates only in colder days.

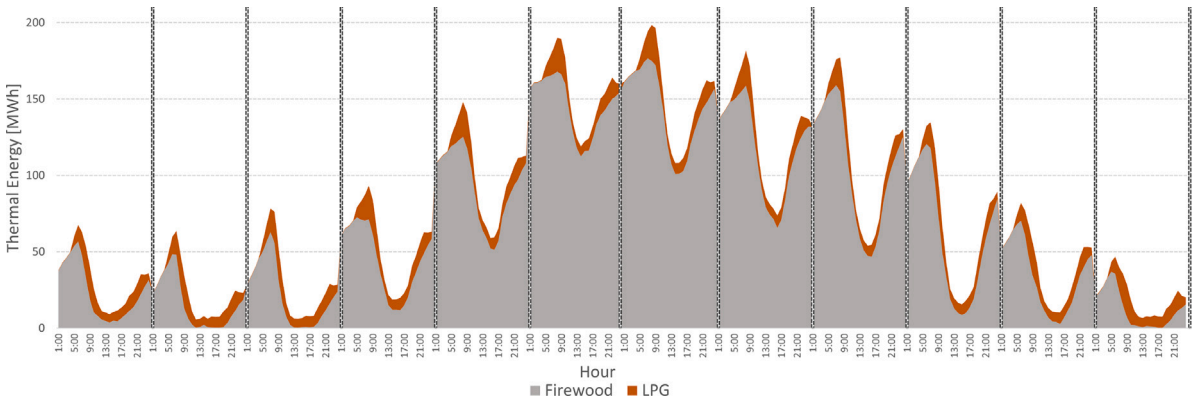

Fig. 8. Annual thermal operation, **Case 0**.

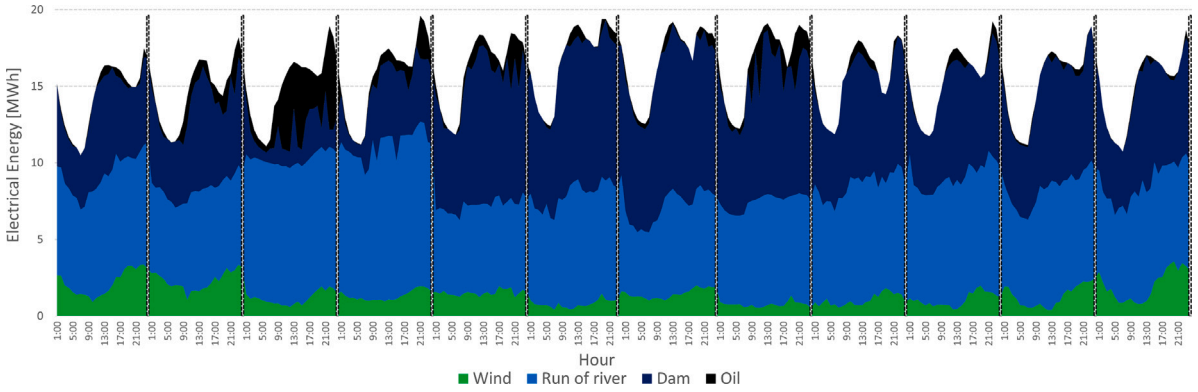

Fig. 9. Annual electrical operation, **Case 0**.

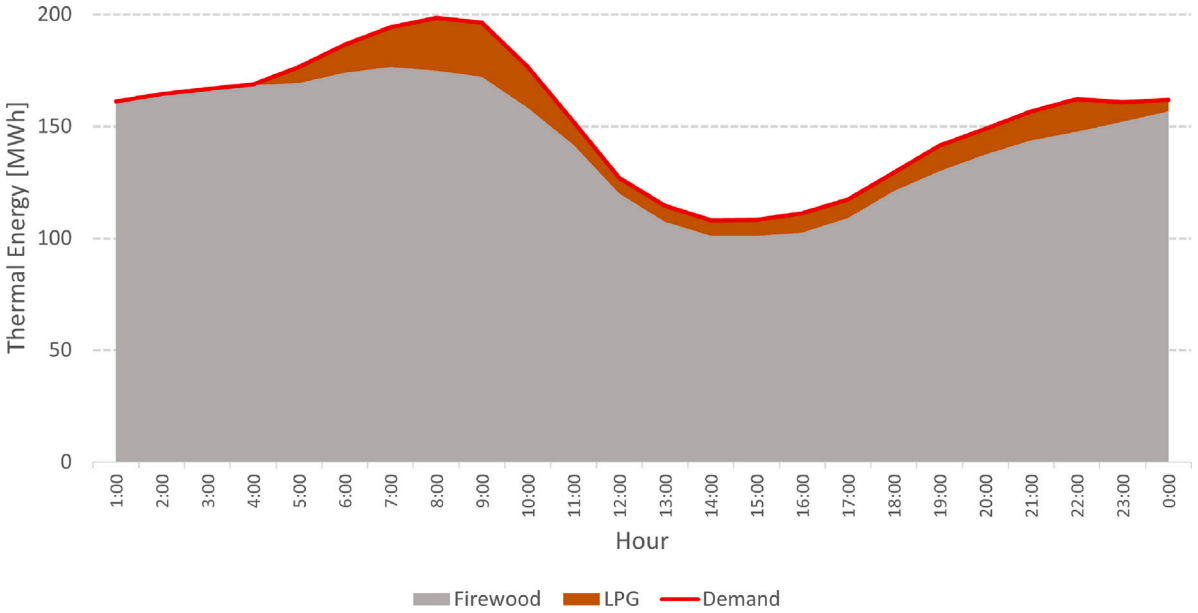

Fig. 10. Thermal operation for typical day in July for worst availability scenario, **Case 0**.

For the worst-day scenario described previously, Fig. 14 shows that electric resistors operate at peak heat demand, while firewood continues to follow its current profile in lower proportion. From the electricity side, Fig. 15 shows that the system's peak electricity demand increases from 20 [MW] previously at midday, to approximately 87 [MW] in the morning hours, evidencing the need for the investment in power lines between zones and within zones described previously. Hydro dam generation operates supplying peak demands, while an

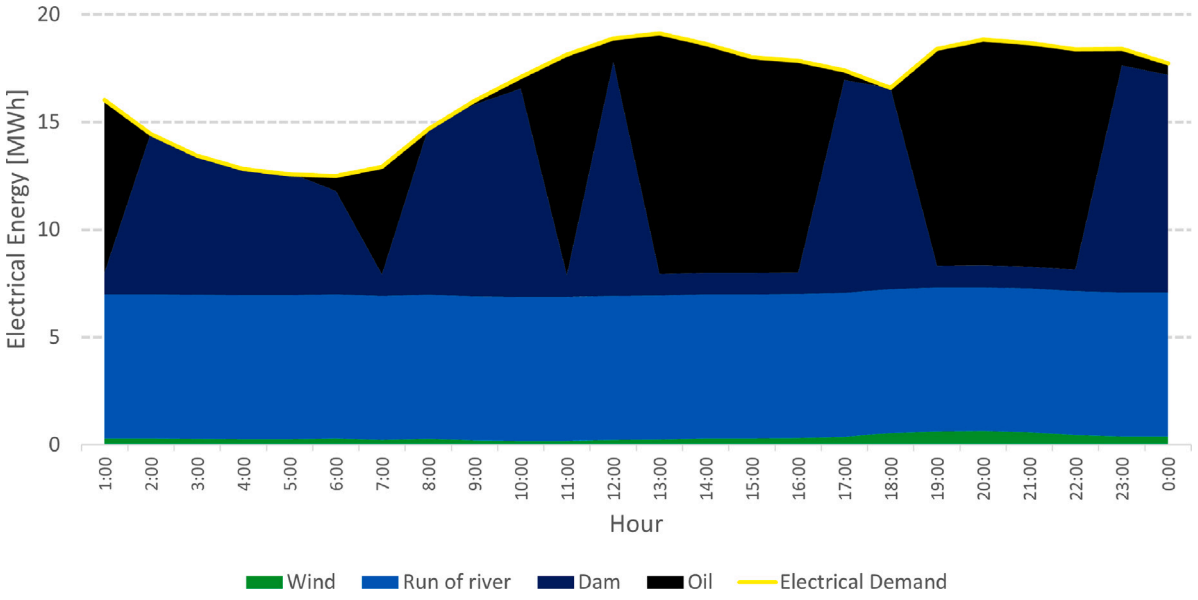

Fig. 11. Electrical operation for typical day in July for worst availability scenario, **Case 0**.

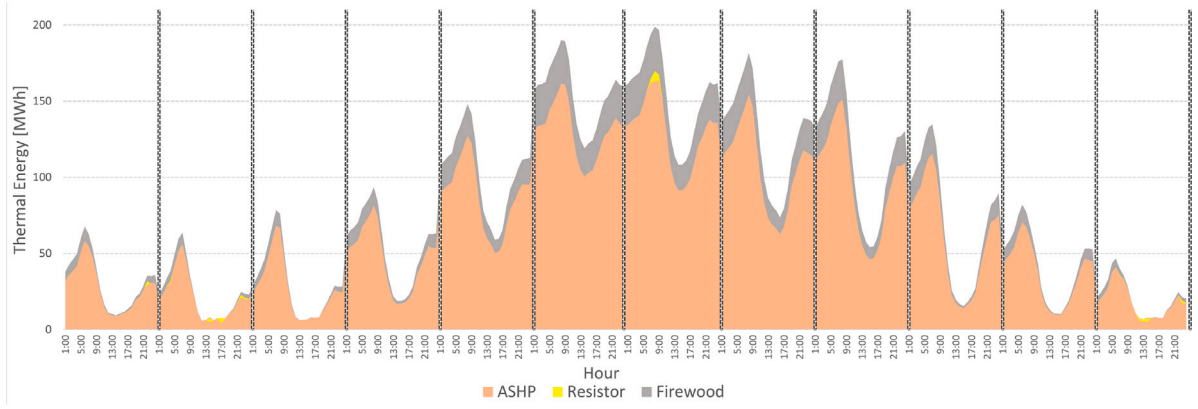

Fig. 12. Annual thermal operation, **Case 3**.

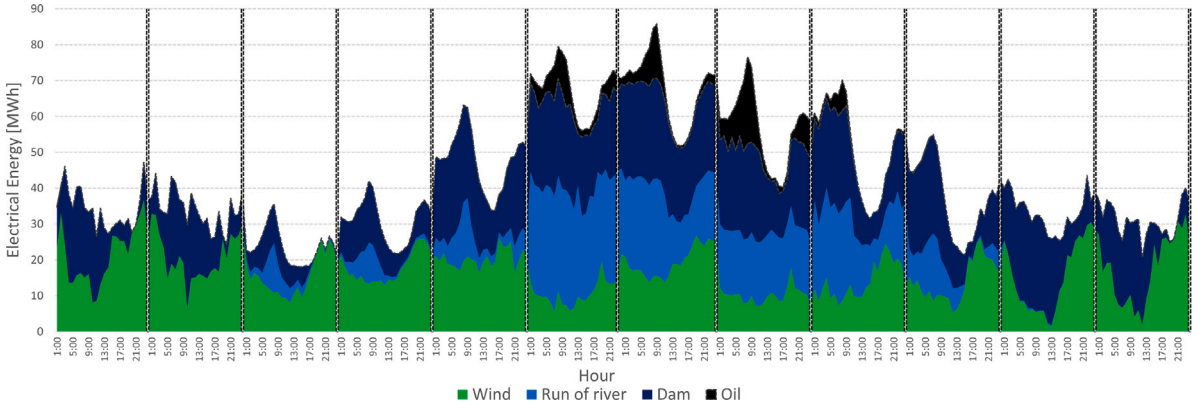

Fig. 13. Annual electrical operation, **Case 3**.

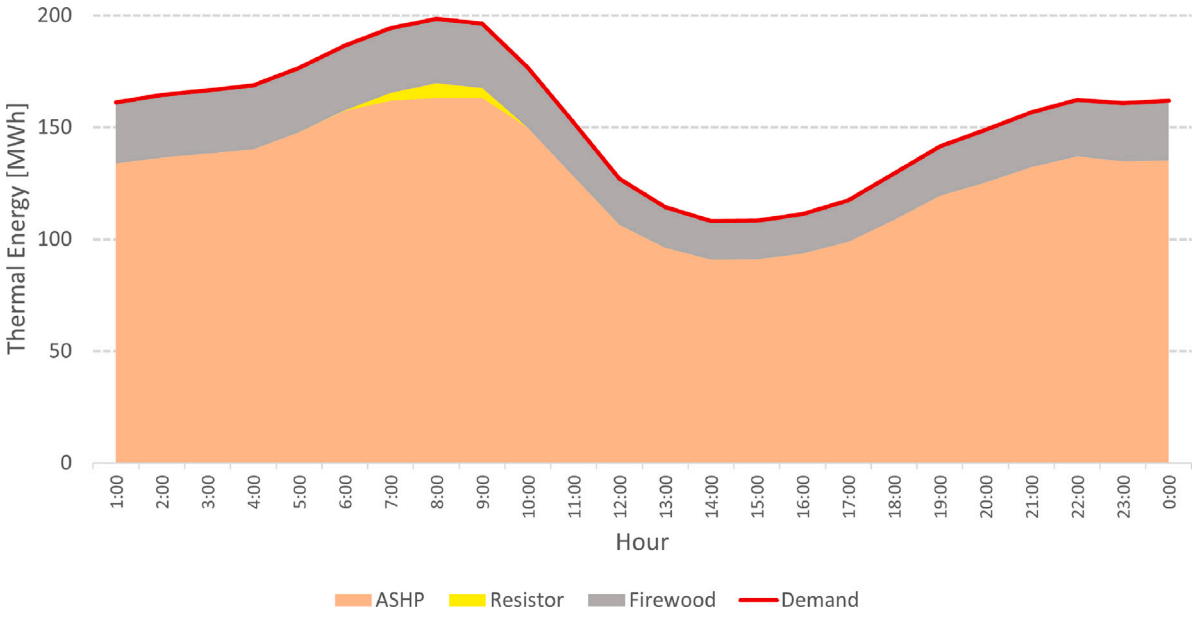

Fig. 14. Thermal operation for typical day in July for worst availability scenario, **Case 3**.

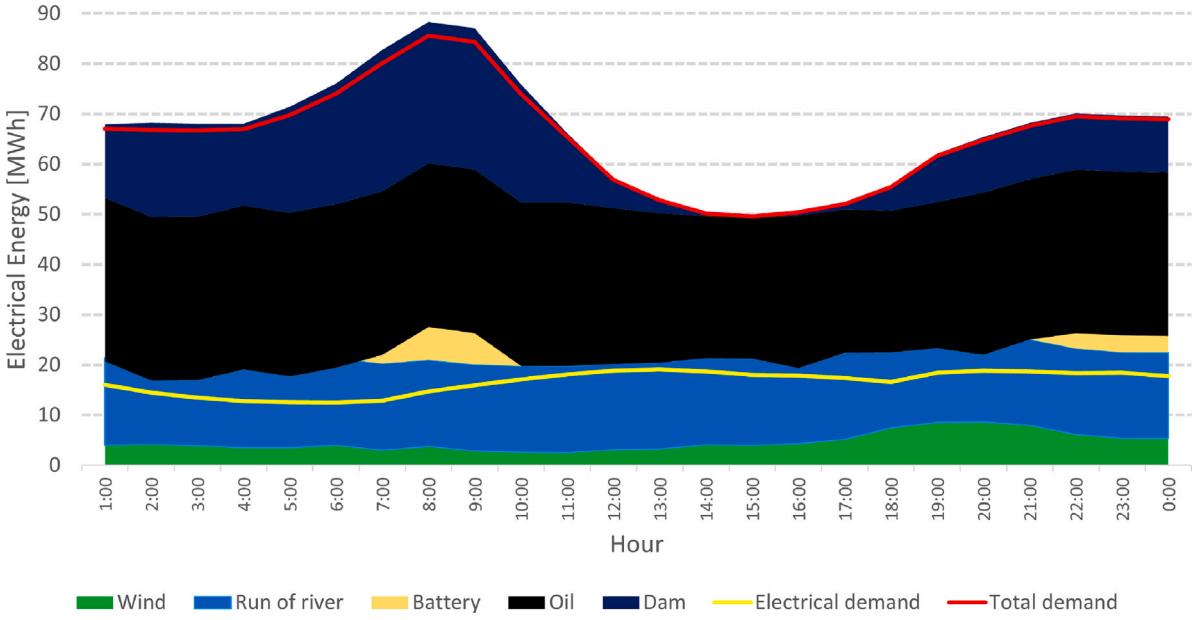

Fig. 15. Electrical operation for typical day in July for worst availability scenario, **Case 3**.

energy arbitrage is performed with batteries, so that they charge in hours with greater availability of wind energy and discharge in hours of higher demands.

4.4. The value of integrated planning

To show the improvement in economic and environmental performances of integrated planning over independent planning of the different energy service demands and vectors, a further case was implemented. This case does not allow investments in expansion of electricity generation, but allows to electrify heat, to invest in electrolysers, in district heating networks. Table 10 shows the costs of integrated planning and heat-only planning for the limits over emissions set in **Case 3**. Under the assumptions and alternatives considered in this work, a heat-vector-only planning results infeasible, as heat requirements would considerably increase electricity demand, which cannot be supplied without expanding electricity generation and without considering non-supplied demand. Although in this case investing in natural gas CHPs is allowed, their associated CO_2 emissions cannot reach the imposed carbon limits.

If the constraint over CO_2 emissions is removed, allowing for a greater deployment of natural gas CHPs and a higher use of existing diesel generation, results presented in Table 11 are obtained. This shows that integrated planning is able to achieve costs and CO_2 emissions reductions when compared to heat-only planning.

4.5. Sensitivity in district heating networks cost

A final set of case studies was implemented with a different cost for district heating networks, as a wide range of values was found in the literature and national studies. This scenario assumed a cost of 335000 [USD/km] for investments in new networks, which represents roughly

Table 10
Integrated planning value.

Planning	Total cost [MMUSD]	NSE [MWh]	NSH [MWh]	PM [ton]	CO_2 [ton]
Heat only	Infeasible	0	0	466	14464
Integrated	53.44	0	0	466	14464

Table 11
Integrated planning value without CO_2 constraints.

Planning	Total cost [MMUSD]	NSE [MWh]	NSH [MWh]	PM [ton]	CO_2 [ton]
Heat only	52.38	0	0	466	154122
Integrated	45.92	0	0	466	64835

Table 12
Low district heat network cost scenario.

	Case 0	Case 1	Case 2	Case 3	Case 4	Case 5
Total cost [MM USD]	18.99	15.99	25.17	50.72	50.71	138.39
Investment cost [MM USD]	0.00	3.09	14.10	47.27	38.02	138.38
Operation cost [MM USD]	18.99	12.90	11.07	3.45	12.69	0.01
Direct CO_2 emissions [ton]	22087	12182	0	11043	85648	0
PM emissions [ton]	2796	2781	2759	466	0	0
Non-supplied energy (electric)	0	0	0	0	0	0
Non-supplied energy (thermal)	0	0	0	0	0	0
CHP [MWth]	0	0	0	0	24.07	0
CHP-H2 [MWth]	0	0	0	0	0	7.42
District ASHP [MWe]	0	7.29	7.58	61.30	53.92	60.22
End-use ASHP [MWe]	0	1.47	1.68	4.85	15.62	15.10
District boilers [MWth]	0	0	0	0	0	0
End-use boilers [MWe]	0	0	0	0	0	0
Electric resistance heater [MWth]	0	1.93	0.6	0.7	0.36	0
Electrolyser [MWe]	0	0	0	0	0	16.16
Hydro dam [MW]	0	0	5.15	18.16	20.44	35.95
Hydro run-of-river [MW]	0	0	11.03	40.94	11.94	95.75
Wind [MW]	0	2.63	21.44	47.65	6.28	323.57
Solar [MW]	0	0	16.20	0	0	7.01
Battery [MW]	0	0	2.04	5.14	6.54	13.03
Total unitary cost [USD/MWh]	23.35	19.66	30.95	62.38	62.37	170.22
Investment unitary cost [USD/MWh]	0.00	3.80	17.34	58.14	46.76	170.21
Operation unitary cost [USD/MWh]	23.35	15.86	13.61	4.24	15.61	0.01
Tariff cost final costumer [USD/MWh]	39.40	35.71	47.00	78.43	78.42	186.30

half of the baseline cost, but is in line with some studies on district heating networks in Chile [54].

The portfolio, along with the same metrics previously discussed, are presented in Table 12 for these case studies. Table 13 presents the investments in networks. While solutions continue to be aimed at heat electrification using heat pumps, in this case which assumes lower costs for district networks, district level ASHPs are seen to predominate over end-use ASHPs. However, in the zone of Puerto Aysén, electrification via end-use ASHPs is still observed, given its low linear heat density compared to other zones. This means that the installation of one kilometre of network in this zone supplies a smaller fraction of peak heat demand than one kilometre of network in Coyhaique or Chacabuco. For these cost parameters, the increase in investment costs for district heating networks over investment in very low voltage electricity networks is lower than the savings generated by installing a district level ASHP over end-use ASHPs. This result, however, depends on the linear heat density within zones as found in previous studies [28].

5. Conclusions

This work presents a novel stochastic multi-energy multi-microgrid system model that optimises investments and operations for integrated electricity, heat and gas isolated energy systems, considering different thermal energy supply routes to displace the use of contaminating fuels. The model includes a fully linear representation of the AC power flow equations, including active and reactive power that are essential in low-voltage networks such as microgrids. Also, the model incorporates firewood as a source of heat (which is the main fuel used in developing countries for heat and cooking) and constraints on the total emissions of CO_2 (for decarbonisation) and particulate matter (for decontamination). Hence, by adjusting the right-hand side of these constraints, we can obtain different designs of the multi-energy multi-microgrid system. To the best of our knowledge, this is the first stochastic planning model with such characteristics.

The model is applied to an isolated region in the south of Chile with an intense use of firewood and liquefied petroleum gas for heating, and a high share of diesel in electricity generation. As the targeted zone is located in Patagonia, the model will attempt to exploit the abundant potential of hydro and wind resources to produce energy.

Firstly, we show that integrated planning leads to an increased economic and environmental performance compared to separate planning of the energy carriers. This is clearly evidenced by comparing the results of the case which represents the current situation (Case 0) and the optimised current situation (Case 1), highlighting that the current situation can be optimised without the need to incorporate emissions constraints. Similarly, when planning the heat-only, and the integrated energy vector for case 3, an increase in economic and environmental performance is observed in the integration.

Under the assumptions used in this case study, the predominant decarbonisation and decontamination alternatives for the provision of heat and electricity service demands are heat pumps, displacing fossil fuels and firewood. As presented in the results, investments in renewables favour the electrification of heat. The sensitivity analysis shows, however, that the costs of district heating networks and linear heat densities will determine if whether the optimal heat electrification strategy is via individual end-use heat pumps, or via district heat pumps supplying district heating networks. For a scenario with lower district

Table 13
Investments in networks for the 6 Cases - low district heat network cost.

Networks between zones (electricity/heat/hydrogen) : 1 if installed, 0 if not						
Line	Case 0	Case 1	Case 2	Case 3	Case 4	Case 5
Chacabuco-Pto Aysén	0/0/0	0/0/0	0/0/0	0/0/0	0/0/0	0/0/1
Pto Aysén-Baguales	0/0/0	0/0/0	0/0/0	0/0/0	0/0/0	0/0/0
Baguales-Tehuelche	0/0/0	0/0/0	0/0/0	1/0/0	0/0/0	1/0/0
Tehuelche-L.Atravesado	0/0/0	0/0/0	0/0/0	1/0/0	1/0/0	1/0/0
Tehuelche-Monreal	0/0/0	0/0/0	0/0/0	1/0/0	0/0/0	1/0/0
Alto Baguales-Villa Ortega	0/0/0	0/0/0	0/0/0	0/0/0	0/0/0	0/0/0
Villa Ortega-Mañihuales	0/0/0	0/0/0	0/0/0	0/0/0	0/0/0	0/0/0
Villa Ortega-Ñirehuao	0/0/0	0/0/0	0/0/0	0/0/0	0/0/0	0/0/0
Networks within zones (electricity/heat/hydrogen): installed km						
Chacabuco	0/0/0	0.72/2.95/0	0/3.67/0	0/30/0	0/30/0	0/30/0
Puerto Aysén	0/0/0	7.34/0/0	7.34/0/0	20.72/0.63/0	59.76/0/0	56.89/3.11/0
Tehuelche	0/0/0	0/11.02/0	0/11.02/0	0/88.55/0	0/90/0	0/90/0
Mañihuales	0/0/0	1.83/0/0	1.83/0/0	1.83/0/0	15/0/0	15/0/0
Ñirehuao	0/0/0	0.73/0/0	0.73/0/0	0.73/0/0	5.34/0/0	6/0/0

heating network infrastructure costs, the investment in district heat pumps dominates, as the difference between electricity distribution networks and district heating networks costs is not sufficient to offset the difference in investment costs between the heat pump options.

Investments in CHPs are only favoured when higher CO_2 emissions are allowed – leading to higher emissions than the current case – which is therefore not aligned with a Net Zero policy. This is also the case for the use of diesel to supply additional electricity requirements for heat electrification. On the other hand, for this case study, investment in hydrogen production and storage technologies was shown to be competitive to supply heat demands only in scenarios with very low/zero CO_2 emissions and particulate matter constraints, taking advantage of the seasonal storage benefit of hydrogen.

The analysis shows that current use of LPG for domestic hot water can be displaced by heat pumps, reducing overall costs, and without the need to impose taxes or limits on CO_2 emissions, through integrated planning. On the other hand, firewood as a heating fuel has a low cost and a high calorific value, which means that it is not naturally displaced by costs, requiring limits on particulate matter, or penalisation through the social cost valuation on people's health. Further alternatives to reduce emissions of particulate matter which were not analysed in this work include additional filters/improved combustion processes for firewood, or subsidies for heat electrification technologies, encouraging end-users to invest in them.

In terms of future work and improvements to the model, we expect to incorporate and evaluate the impact of low-regret measures such as energy efficiency measures – e.g. thermal insulation in homes, more efficient wood-stoves – particle filters, and improved firewood quality. In terms of network representation, future work includes considering more details in power system operation such as active power reserve constraints for primary and secondary frequency control, as well as optimal demand response mechanisms.

CRediT authorship contribution statement

Claudio Carvallo: Conceptualization, Data curation, Methodology, Formal analysis, Writing – original draft. **Francisca Jalil-Vega:** Supervision, Writing – original draft. **Rodrigo Moreno:** Funding acquisition, Supervision, Writing – review & editing.

Data availability

Data will be made available on request.

Acknowledgements

This research was supported by ANID through Instituto Sistemas Complejos de Ingeniería ANID PIA/PUENTE AFB220003, by EPSRC through Supergen Energy Networks Hub EP/S00078X/2, and by ANID through grants FONDECYT N.1231924, FONDECYT N.1181928, PIA-ACT-192094, FONDECYT N.11220388, FONDEF ID21I10119, ANID/FONDAP/15110019 SERC-Chile, and ANID/Millennium Scientific Initiative of the Ministry of Science, Technology, Knowledge, and Innovation/ICN2021_023 (MIGA).

Appendix A. Nomenclature

A.1. List of acronyms

$ASHP$	Air-source heat pumps (end-use in model formulation)
Aux	Electric resistor heater
BS	Battery storage
CHP	Gas-fuelled CHP
Dam	Hydro dam
DHW	Domestic hot water
EHB	End-use hydrogen boiler
NSE	Non-supplied energy
FW	Firewood end-use heating
LPG	Liquefied petroleum gas end-use
LNG	Liquefied natural gas for CHP
HB	District level hydrogen boiler
$HCHP$	Hydrogen-fuelled CHP
HP	District level air-source heat pumps
HS	Hydrogen storage
HT	Space-heating
Oil	Diesel
PV	Photovoltaic
$P2G$	Electrolyser
ROR	Hydro run-of-river
WT	Wind turbine

A.2. Sets and elements

$c \in C$	Element and set of fuels: FW, LPG, LNG, Oil.
$d \in D$	Element and set of typical days.
$g \in G$	Element and set of electricity generators.
$h \in H$	Element and set of heat generators.
$j \in \bar{J}$	Element and set of hot water pipes between zones.
$k \in \bar{K}$	Element and set of hydrogen pipes between zones.
$l \in \bar{L}$	Element and set of low voltage lines between zones.
$n \in N$	Element and set of zones.
$p \in P$	Element and set of heat demands: space-heating (HT), hot water (DHW), and total heat (TOT).
$r \in R \subset G$	Element and set of renewable generation technologies.
$t \in T$	Element and set hours.
$s \in S$	Element and set of scenarios.

A.3. Parameters

Parameter	Description	Units
B_n^{sh}	Susceptance in zone n	S
COP_t	Coefficient of performance of air-source heat pumps in hour t	–
CE_c	CO_2 emission factor of fuel c	tonCO_2/MWh
CET	Annual CO_2 emission limit	tonCO_2
PMT	Annual particulate matter emission limit	tonMP2.5
D_j^{HN}	Hot water pipe j length to be installed (between zones)	km
D_k^{GN}	hydrogen pipe k length to be installed (between zones)	km
H_n^{max}	Peak heat demand in zone n	MW
$H_{n,t}^{D}$	Total heat demand in zone n, in hour t	MW
$H_{n,t}^{DFW}$	Heat demand supplied by firewood in zone n, in hour t	MW
$H_{n,t}^{DLPG}$	Heat demand supplied by LPG in zone n, in hour t	MW
$h_{p,n,t}$	Normalised demand profile of heat demand type p, in zone n and hour t	%
HV^{LNG}	High heating value of natural gas	kcal/kg
HV^{H_2}	High heating value of hydrogen	kcal/kg
$\overline{I}_{m,n}$	Maximum current capacity of line that connects zones m and n	A
Km_n	Total road length in zone n	km
N_d^{Days}	Number of days represented by typical day d	
$\overline{L}^{H2,vol}$	Volumetric percentage limit of hydrogen in hydrogen-natural gas blend	%
N^{CHP}	Availability factor CHP	%
$P_{n,t}^{D}$	Active power demand in zone n and hour t	MW
$PF_{n,s,d}^{Dam}$	Plant factor of reservoir in zone n, in scenario s, in typical day d	%
PM^{FW}	Emission factor of particulate matter 2.5 associated to firewood use	kgPM2.5/m^3
$\tilde{P}_{m,n}$	Feasible predicted operating point of active power for the line that connects zones m and n	MW
$\tilde{Q}_{m,n}$	Feasible predicted operating point of reactive power for the line that connects zones m and n	MVAr
$Q_{n,t}^{D}$	Reactive power demand in zone n in hour t	MW
R_g	Ramp rate of generator g.	MW/h
$R_{m,n}$	Resistance of line that connects zones m and n	Ohm
$X_{m,n}$	Reactance of line that connects zones m and n	Ohm
$\overline{S}_{m,n}$	Aparent capacity of electric line between zones m and n	MVA
$\overline{V}$, $\underline{V}$	Maximum and minimum voltage values in each zone for electric network	V
$\alpha_{r,s,t}$	Availability of renewable resource r in scenario s and hour t	%
η^{eCHP}	CHP electric efficiency	%
η^{hCHP}	CHP thermal efficiency	%
η_h	Thermal efficiency of technology h	%
η^{loss}	Self-discharge fraction of hydrogen storage	%
η^{P2G}	Electrolyser efficiency	%
η^{BS}	Batteries charging efficiency	%
η^{HS}	Charging efficiency of hydrogen storage	%
π^{FW}	Firewood cost	USD/MWh
π^{LPG}	LPG cost	USD/MWh
π^{LNG}	LNG cost	USD/MWh
π^{HLL}	Cost of non-supplied thermal energy	USD/MWh
π^{kmDx}	Annualised investment cost of very low voltage line per kilometre	USD/km/year
π^{kmHN}	Annualised investment cost of district heating network per kilometre	USD/km/year
π^{kmGN}	Annualised investment cost of hydrogen network per kilometre	USD/km/year
π^{IGN}	Annualised investment cost of gas network per kilometre	USD/km/year
π_g^{I}	Annualised investment cost of electricity generation technology g	USD/MW/year
π_h^{I}	Annualised investment cost of heat generation technology g	USD/MW/year
π^{IHN}	Annualised investment cost of district heating network between zones	USD/km/MW/year
π_l^{I}	Annualised investment cost of low voltage reinforcement line l	USD/year
π^{IP2G}	Annualised investment cost of electrolyser	USD/MW/year
π^{IBS}	Annualised investment cost of batteries	USD/MW/year
π^{IHS}	Annualised investment cost of hydrogen storage USD/MW/year	
π_g^{O}	Variable cost of generation technology g	USD/MW
π^{PLL}	Non-supplied electricity cost	USD/MW
ρ_s	Probability of occurrence of scenario s	%
τ^{BS}	Battery storage duration	h
τ^{HS}	Hydrogen storage duration	h

A.4. Variables

Variable	Description	Units
$C_{n,s,t}^{FW}$	Firewood consumption in zone n, scenario s, and hour t	MW
$C_{n,s,t}^{LPG}$	LPG consumption in zone n, scenario s, and hour t	MW
$f_{k,s,t}^{gas}$	Gas flow transported in pipeline k, in scenario s, and hour t	MW
$\overline{F}_k^{gas}$	Hydrogen pipeline k capacity	MW
$f_{j,s,t}^{heat}$	Heat flow transported in pipeline j, in scenario s, and hour t	MW
$\overline{F}_j^{heat}$	Capacity of heat pipeline j	MW
$G_{n,s,t}^{LNG}$	Natural gas consumed by CHP in zone n, scenario s, and hour t	MW
$G_{h,n,s,t}$	Hydrogen consumed by technology h, in zone n, scenario s, and hour t	MW
$G_{n,s,t}^{P2G}$	Hydrogen produced by electrolyser in zone n, scenario s, and hour t	MW
$G_{n,s,d}^{HSE_0}$	Hydrogen stored at the beginning of typical day d, in zone n, scenario s, and hour t	MWh
$H_{h,n,s,t}$	Thermal power generated by technology h in zone n, scenario s, and hour t	MW
$H_{n,s,t}^{endu}$	Heat demand supplied by end-use technologies (other than district heating networks) in zone n, scenario s, and hour t	MW

(continued on next page)

Variable	Description	Units
$H^{dhn}_{n,s,t}$	Heat demand supplied by district heating networks in zone n, in scenario s, and hour t	MW
$\overline{H}_{h,n}$	Thermal capacity of technology h in zone n	MW
Inv	Investment cost	USD
$i_{m,n,s,t}$	Quadratic current variable between zones m and n, in scenario s, and hour t	A^2
Km^{Dx}_n	Low voltage network length to be installed in zone n	km
Km^{GN}_n	Hydrogen network length to be installed in zone n	km
Km^{HN}_n	District heating network length to be installed in zone n	km
OF	Objective function	USD
$Ope_{s,t}$	Operation cost in scenario s and hour t	USD
$P_{n,s,t}$	Net active power in zone n, in scenario s, and hour t	MW
$Q_{n,s,t}$	Net reactive power in zone n, in scenario s, and hour t	MVAr
$P_{h,n,s,t}$	Electricity consumption of technology h, in zone n, in scenario s, and hour t	MW
$P^{P2G}_{n,s,t}$	Electricity consumption of electrolyser in zone n, in scenario s, and hour t	MW
$P_{g,n,s,t}$	Active power generated by technology g in zone n, in scenario s, and hour t	MW
$Q_{g,n,s,t}$	Reactive power generated by technology g in zone n, in scenario s, and hour t	MVAr
$\overline{P}_{g,n}$	Electric capacity of generator g in zone n	MW
$H^{LL}_{n,s,t}$	Non-supplied electricity demand in zone n, in scenario s, and hour t	MW
$P^{LL}_{n,s,t}$	Non-supplied heat demand in zone n, in scenario s, and hour t	MW
$P_{m,n,s,t}$	Active power in the line connecting zones m and n, in scenario s and hour t	MW
$Q_{m,n,s,t}$	Reactive power in the line connecting zones m and n, in scenario s and hour t	MVAr
$\overline{P}^{P2G}_n$	Electric capacity of electrolyser in zone n	MW
$P^{HS}_{n,s,t}$	Net power of hydrogen storage technology in zone n, in scenario s, and hour t	MW
$P^{HS+}_{n,s,t}$	Charging power of hydrogen storage technology in zone n, in scenario s, and hour t	MW
$P^{HS-}_{n,s,t}$	Discharging power of hydrogen storage technology in zone n, in scenario s, and hour t	MW
$P^{BS}_{n,s,t}$	Net power of battery storage in zone n, in scenario s, and hour t	MW
$P^{BS+}_{n,s,t}$	Charging power of battery storage in zone n, in scenario s, and hour t	MW
$P^{BS-}_{n,s,t}$	Discharging power of battery storage in zone n, in scenario s, and hour t	MW
$P^{HSE}_{n,s,t}$	Energy stored by hydrogen storage technology in zone n, in scenario s, and hour t	MWh
$P^{BSE}_{n,s,t}$	Energy stored by battery storage in zone n, in scenario s, and hour t	MWh
$Q^{BS}_{n,s,t}$	Reactive power injected by battery storage in zone n, scenario s, and hour t	MVAr
$\overline{P}^{BS}_n$	Battery storage in zone n	MW
$\overline{P}^{HS}_n$	Hydrogen storage capacity in zone n	MW
$v_{n,s,t}$	Quadratic voltage variable in the bar associated to zone n, in scenario s, and hour t	V^2
μ_l	Binary variable equal to 1 if the low voltage line l is reinforced, and 0 otherwise	–

Appendix B. Full model formulation

B.1. Objective function

The objective function (Eq. (B.1)) minimises the annualised investment cost and expected operating cost.

$$OF = \min \left\{ Inv + \sum_{s\in S}\sum_{t\in T} \rho_s Ope_{s,t} \right\} \tag{B.1}$$

The total investment costs include the costs of all networks and technologies (Eq. (B.2)):

$$\begin{aligned} Inv = & \sum_{h\in H, n\in N} \pi^I_h \overline{H}_{h,n} + \sum_{g\in G, n\in N} \pi^I_g \overline{P}_{g,n} + \sum_{n\in N} \pi^{IBS} \overline{P}^{BS}_n \\ & + \sum_{n\in N} \pi^{IHS} \overline{P}^{HS}_n + \sum_{n\in N} \pi^{IP2G} \overline{P}^{P2G}_n \\ & + \sum_{n\in N} \pi^{kmDx} Km^{Dx}_n + \sum_{n\in N} \pi^{kmHN} Km^{HN}_n + \sum_{n\in N} \pi^{kmGN} Km^{GN}_n \\ & + \sum_{j\in \bar{J}} \pi^{IHN} D^{HN}_j \overline{F}^{heat}_j + \sum_{k\in \bar{K}} \pi^{IGN} D^{GN}_k \overline{F}^{gas}_k + \sum_{l\in \bar{L}} \pi^I_l \mu_l \end{aligned} \tag{B.2}$$

Operating costs (Eq. (B.3)) are made up of the variable costs of electrical generators, fuel consumption costs, and non-supplied energy costs for both heat and electricity.

$$\begin{aligned} Ope_{s,t} = & \sum_{n\in N, g\in G} \pi^O_g P_{g,n,s,t} + \sum_{n\in N} \pi^{LPG} C^{LPG}_{n,s,t} + \sum_{n\in N} \pi^{FW} C^{FW}_{n,s,t} \\ & + \sum_{n\in N} \pi^{LNG} G^{LNG}_{n,s,t} + \sum_{n\in N} \pi^{PLL} P^{LL}_{n,s,t} + \sum_{n\in N} \pi^{HLL} H^{LL}_{n,s,t}; \\ & \forall s\in S, t\in T \end{aligned} \tag{B.3}$$

B.2. Energy balance equations

The balance of electricity is shown in Eq. (B.4). Eq. (B.5) indicates that the net reactive power in each zone is equal to the reactive demand in the zone minus the reactive injection by the generators and batteries.

$$P_{n,s,t} = P^D_{n,t} + \sum_{h\in\{Aux,HP,ASHP\}} P_{h,n,s,t} + P^{P2G}_{n,s,t} - P^{LL}_{n,s,t} - P^{BS}_{n,s,t} - \sum_{g\in G} P_{g,n,s,t}; \quad \forall n\in N, s\in S, \forall t\in T \tag{B.4}$$

$$Q_{n,s,t} = Q^D_{n,t} - Q^{BS}_{n,s,t} - \sum_{g\in G} Q_{g,n,s,t}; \qquad \forall n\in N, \forall s\in S, \forall t\in T \tag{B.5}$$

Eq. (B.8) shows the heat balance equation, where heat demand can be supplied either by a district heating network, or by individual end-use technologies (Eq. (B.7)).

$$H^D_{n,t} - H^{LL}_{n,s,t} = H^{dhn}_{n,s,t} + H^{endu}_{n,s,t}; \qquad \forall n\in N, \forall s\in S, \forall t\in T \tag{B.6}$$

$$H^{endu}_{n,s,t} = \sum_{h\in\{ASHP,FW,EHB,aux,LPG\}} H_{h,n,s,t}; \qquad \forall n\in N, \forall s\in S, \forall t\in T \tag{B.7}$$

In the district energy balance equation, bi-directional exchange of energy flows between two locations is allowed, as shown in Eq. (B.8). Such flows cannot exceed the capacity of the thermal link (Eq. (B.9)).

$$H^{dhn}_{n,s,t} = \sum_{h\in\{CHP,HCHP,HB,HP\}} H_{h,n,s,t} + \sum_{j\in From_n} f^{heat}_{j,s,t} - \sum_{j\in To_n} f^{heat}_{j,s,t}; \quad \forall n\in N, \forall s\in S, \forall t\in T \tag{B.8}$$

$$-\overline{F}^{heat}_{j} \le f^{heat}_{j,s,t} \le \overline{F}^{heat}_{j}; \qquad \forall j\in \bar{J}, \forall s\in S, \forall t\in T \tag{B.9}$$

Eq. (B.10) shows the hydrogen balance equation:

$$G^{P2G}_{n,s,t} + P^{HS}_{n,s,t} = \sum_{h\in\{CHP,EHB,HCHP,HB\}} G_{h,n,s,t} + \sum_{k\in From_n} f^{gas}_{k,s,t} - \sum_{k\in To_n} f^{gas}_{k,s,t}; \quad \forall n\in N, \forall s\in S, \forall t\in T \tag{B.10}$$

Exchange of gas flows between zones is allowed, subject to the maximum capacity of pipelines to be installed, according to Eq. (B.11).

$$-\overline{F}^{gas}_{k} \le f^{gas}_{k,s,t} \le \overline{F}^{gas}_{k}; \qquad \forall k\in \bar{K}, \forall s\in S, \forall t\in T \tag{B.11}$$

B.3. Flows in low voltage networks

The following formulation of AC power flows in the low voltage networks connecting cities and generation points is proposed, based on quadratic variables for voltage ($v_{n,s,t}$) in each zone (Eq. (B.12)), and current in each network line ($i_{m,n,s,t}$) (Eq. (B.13)).

$$v_{n,s,t} = |V_{n,s,t}|^2; \qquad \forall n\in N, \forall s\in S, \forall t\in T \tag{B.12}$$

$$i_{m,n,s,t} = |I_{m,n,s,t}|^2; \qquad \forall (m,n)\in N\times N, \forall s\in S, \forall t\in T \tag{B.13}$$

The voltage in each zone is bounded by a minimum and a maximum value (Eq. (B.14)), while current in each line is limited to the line's maximum current capacity (Eq. (B.15)).

$$\underline{V}^2 \le v_{n,s,t} \le \overline{V}^2; \qquad \forall n\in N, \forall s\in S, \forall t\in T \tag{B.14}$$

$$i_{m,n,s,t} \le \overline{I}^2_{m,n}; \qquad \forall (m,n)\in N\times N, \forall s\in S, \forall t\in T \tag{B.15}$$

Eq. (B.16) relates the voltages between two consecutive zones, by the flows and losses of active and reactive power passing through the line that connects them, and its electrical parameters.

$$v_{n,s,t} = v_{m,s,t} - 2(R_{m,n}P_{m,n,s,t} + X_{m,n}Q_{m,n,s,t}) + i_{m,n,s,t}(R^2_{m,n} + X^2_{m,n}); \quad \forall (m,n)\in N\times N, \forall s\in S, \forall t\in T \tag{B.16}$$

Eq. (B.17) defines the active power flow through the line connecting zones m and n, while Eq. (B.18) defines the reactive power flow in the line connecting two zones.

$$P_{m,n,s,t} = P_{n,s,t} + R_{m,n}i_{m,n,s,t} + \sum_{fr\ n=i} P_{i,j,s,t} - \sum_{to\ n=j} P_{i,j,s,t}; \quad \forall (m,n)\in N\times N, \forall s\in S, \forall t\in T \tag{B.17}$$

$$Q_{m,n,s,t} = Q_{n,s,t} + X_{m,n}i_{m,n,s,t} + B^{sh}_{n}v_{n,s,t} + \sum_{fr\ n=i} Q_{i,j,s,t} - \sum_{to\ n=j} Q_{i,j,s,t}; \quad \forall (m,n)\in N\times N, \forall s\in S, \forall t\in T \tag{B.18}$$

The formulation is completed by the following non-linear equations: Eq. (B.19) models the apparent power capacity of the lines, while Eq. (B.20) relates the power flows to the voltage in the emitter zone and current in the line.

$$P^2_{m,n,s,t} + Q^2_{m,n,s,t} \le \overline{S}^2_{m,n}; \qquad \forall (m,n)\in N\times N, \forall s\in S, \forall t\in T \tag{B.19}$$

$$v_{n,s,t}\cdot i_{m,n,s,t} \ge P^2_{m,n,s,t} + Q^2_{m,n,s,t}; \qquad \forall (m,n)\in N\times N, \forall s\in S, \forall t\in T \tag{B.20}$$

Eqs. (B.19) and (B.20) are approximated to linear Eqs. (B.21) and (B.22), respectively, by means of tangent lines and planes.

$$-\frac{-\alpha P_{m,n,s,t} + \overline{S}_{m,n}}{\sqrt{1-\alpha^2}} \le Q_{m,n,s,t} \le \frac{-\alpha P_{m,n,s,t} + \overline{S}_{m,n}}{\sqrt{1-\alpha^2}}; \quad \forall (m,n)\in N\times N, \forall s\in S, \forall t\in T, \forall \alpha\in(-1,1) \tag{B.21}$$

$$\tilde{V}_n i_{m,n,s,t} \ge \tilde{P}^2_{m,n} + \tilde{Q}^2_{m,n} + 2\tilde{P}_{m,n}(P_{m,n,s,t} - \tilde{P}_{m,n}) + 2\tilde{Q}_{m,n}(Q_{m,n,s,t} - \tilde{Q}_{m,n}); \quad \forall (m,n)\in N\times N, \forall s\in S, \forall t\in T \tag{B.22}$$

Note that the region defined by the right-hand side of Eq. (B.22) corresponds to the linear approximation of the region defined by the right-hand side of Eq. (B.20) via supporting planes. This approximation is possible because Eq. (B.20) is convex if we assume that $\tilde{V}_n = 1[p.u.]$. Note also that $\tilde{P}_{m,n}$ and $\tilde{Q}_{m,n}$ can represent different predefined points that seek to discretise the $P-Q$ space. $\tilde{P}_{m,n}$ and $\tilde{Q}_{m,n}$ should be selected such that:

$$\tilde{P}^2_{m,n} + \tilde{Q}^2_{m,n} \le \overline{S}^2_{m,n} \qquad \forall (m,n)\in N\times N \tag{B.23}$$

B.4. Energy distribution networks

For district heating networks, the sum of the capacities of technologies connected to the network must be less than or equal to the fraction of the maximum demand of the area that will be supplied by this route [27], as shown in Eq. (B.24).

$$\sum_{h\in\{HP,CHP,HB,HCHP\}} \overline{H}_{h,n} \le Km^{HN}_{n}\frac{H^{max}_{n}}{Km_{n}}; \qquad \forall n\in N \tag{B.24}$$

Similarly, the sum of the capacities of technologies that connect to the low-voltage grid must be less than or equal to the fraction of demand that will be supplied by these technologies. The decision variable represents the kilometres of low-voltage grid that need to be reinforced due to the incorporation of these new electrical loads (Eq. (B.25)).

$$\sum_{h\in\{ASHP,Aux\}} \overline{H}_{h,n} \le Km^{Dx}_{n}\frac{H^{max}_{n}}{Km_{n}}; \qquad \forall n\in N \tag{B.25}$$

The same is used for hydrogen networks (Eq. (B.26)):

$$\overline{H}_{h=EHB,n} \le Km^{GN}_{n}\frac{H^{max}_{n}}{Km_{n}}; \qquad \forall n\in N \tag{B.26}$$

B.5. Thermal power generation

Thermal power delivered by air-source heat pumps is equal to the electrical power consumed, multiplied by their COP (Eq. (B.27)), and is subject to their maximum capacity (Eq. (B.28)).

$$H_{h,n,s,t} = P_{h,n,s,t}COP_{t}; \qquad \forall h\in\{ASHP,HP\}, \forall n\in N, \forall s\in S, \forall t\in T \tag{B.27}$$

$$H_{h,n,s,t} \le \overline{H}_{h,n}; \qquad \forall h\in\{ASHP,HP\}, \forall n\in N, \forall s\in S, \forall t\in T \tag{B.28}$$

The thermal power delivered by hydrogen boilers is equal to the hydrogen consumed – in terms of its heating value – times the boilers' efficiency (Eq. (B.29)), and is also subject to their maximum capacity (Eq. (B.30)).

$$H_{h,n,s,t} = G_{h,n,s,t}\eta_{h}; \qquad \forall h\in\{EHB,HB\}, \forall n\in N, \forall s\in S, \forall t\in T \tag{B.29}$$

$$H_{h,n,s,t} \le \overline{H}_{h,n}; \qquad \forall h\in\{EHB,HB\}, \forall n\in N, \forall s\in S, \forall t\in T \tag{B.30}$$

Two types of CHPs are also incorporated; a hybrid CHP fuelled by natural gas/hydrogen mixtures, and a CHP fuelled by pure hydrogen. Their thermal power production is bounded by their maximum thermal capacity and weighted by an availability factor which accounts for annual maintenance periods as shown in Eq. (B.31).

$$H_{h,n,s,t} \leq N^{CHP}\overline{H}_{h,n}; \quad \forall h \in \{HCHP, CHP\}, \forall n \in N, \forall s \in S, \forall t \in T \tag{B.31}$$

Eqs. (B.32) and (B.33) state that generated electrical and thermal power equate to the primary fuel consumption weighted by the CHP's electrical and thermal efficiencies, respectively.

$$P_{g,n,s,t} = (G^{LNG}_{n,s,t} + G_{h,n,s,t})\eta^{eCHP}; \quad \forall g \in \{HCHP, CHP\}, h \in \{CHP\}, \forall n \in N, \forall s \in S, \forall t \in T \tag{B.32}$$

$$H_{h,n,s,t} = (G^{LNG}_{n,s,t} + G_{h,n,s,t})\eta^{hCHP}; \quad \forall h \in \{CHP\}, \forall n \in N, \forall s \in S, \forall t \in T \tag{B.33}$$

Eq. (B.34) states that generation between one hour and the next cannot be greater than a maximum load shedding or load shedding ramp.

$$-R_g\overline{H}_{h,n} \leq H_{h,n,s,t-1} - H_{h,n,s,t} \leq R_g\overline{H}_{h,n}; \quad \forall g \in \{CHP\}, \forall h \in \{CHP\}, \forall n \in N, \forall s \in S, \forall t \in T \tag{B.34}$$

Finally, in the case of hybrid CHPs, the hydrogen present in the mixture cannot exceed a maximum percentage in volume as shown in Eq. (B.35). As the limit expressed in volume percentage, Eq. (B.36) converts the limit into energy units.

$$G_{h,n,s,t} \leq \overline{L}^{H_2,energy}(G_{h,n,s,t} + G^{LNG}_{n,s,t}); \quad h \in \{CHP\}, \forall n \in N, \forall s \in S, \forall t \in T \tag{B.35}$$

$$\overline{L}^{H_2,energy} = \frac{\overline{L}^{H_2,vol} HV^{H_2}}{(1-\overline{L}^{H_2,vol})HV^{LNG} + \overline{L}^{H_2,vol} HV^{H_2}} \tag{B.36}$$

B.6. Hydrogen generation and storage

The hydrogen produced by the electrolyser is the active power consumed times a conversion efficiency (Eq. (B.37)). Its power consumption is limited to the electrical capacity of the electrolyser (Eq. (B.38)).

$$G^{P2G}_{n,s,t} = P^{P2G}_{n,s,t}\eta^{P2G}; \quad \forall n \in N, \forall s \in S, \forall t \in T \tag{B.37}$$

$$P^{P2G}_{n,s,t} \leq \overline{P}^{P2G}_{n}; \quad \forall n \in N, \forall s \in S, \forall t \in T \tag{B.38}$$

Hydrogen storage is represented through a series of constraints. Eqs. (B.39) and (B.40) state that the net charging power (discharge minus charging) is bounded by the storage tank's charging capacity, for the entire set of hours within each representative day. The energy contained in the tank cannot be greater than the maximum charging power multiplied by the duration of the storage in hours (Eq. (B.41)). Within each representative day and from the second hourly block onwards, the energy contained in a given hour is calculated as the energy contained in the previous hour, plus the load, and minus the discharge in the current hour, as shown in Eq. (B.42).

$$P^{HS}_{n,s,t} = P^{HS-}_{n,s,t} - P^{HS+}_{n,s,t}; \quad \forall n \in N, \forall s \in S, \forall t \in T \tag{B.39}$$

$$-\overline{P}^{HS}_{n} \leq P^{HS}_{n,s,t} \leq \overline{P}^{HS}_{n}; \quad \forall n \in N, \forall s \in S, \forall t \in T \tag{B.40}$$

$$P^{HSE}_{n,s,t} \leq \overline{P}^{HS}_{n}\tau^{HS}; \quad \forall n \in N, \forall s \in S, \forall t \in T \tag{B.41}$$

$$P^{HSE}_{n,s,t} = P^{HSE}_{n,s,t-1} - P^{HS-}_{n,s,t} + P^{HS+}_{n,s,t}\eta^{HS}; \quad \forall d \in D, \forall n \in N, \forall s \in S, \forall t \in \{24(d-1)+2, \ldots, 24d\} \tag{B.42}$$

The initial condition $G^{HSE_0}_{d}$ for each representative day (except the first), is calculated as a function of the initial condition and the state of charge in the 24th hour of the previous representative day, as shown in Eq. (B.43).

$$G^{HSE_0}_{n,s,d} = (1-\eta^{loss}) \cdot (G^{HSE_0}_{n,s,d-1} + N^{days}_{d} \cdot (P^{HSE}_{n,s,t=24d} - G^{HSE_0}_{n,s,d-1})); \quad \forall d \in D, \forall n \in N, \forall s \in S \tag{B.43}$$

The energy in the first hour of each representative day is given by the initial condition described above, plus the net charge during the first hour (Eq. (B.44)).

$$P^{HSE}_{n,s,t=24(d-1)+1} = G^{HSE_0}_{n,s,d} - P^{HS-}_{n,s,t=24(d-1)+1} + P^{HS+}_{n,s,t=24(d-1)+1}\eta^{HS}; \quad \forall d \in D, \forall n \in N, \forall s \in S \tag{B.44}$$

Finally, the energy at the 24th hour of the last representative day must be equal to the initial energy of the first day, in this case zero (Eq. (B.45)).

$$P^{HSE}_{n,s,t=1} = P^{HSE}_{n,s,t=Card(D)\cdot 24} = 0; \quad \forall n \in N, \forall s \in S \tag{B.45}$$

B.7. Electricity generation and storage

Eq. (B.46) shows the end-point model for plants with regulation capacity.

$$\sum_{t \in T_d} P_{g,n,s,t} \leq \overline{P}_{g,n} PF^{Dam}_{n,s,d} Card(T_m); \quad \forall d \in D, \forall g \in \{Dam\}, \forall n \in N, \forall s \in S \tag{B.46}$$

For non-dispatchable renewable power plants, power generated in each hour cannot exceed the plant's capacity times the availability factor in that hour, as shown in (B.47).

$$P_{r,n,s,t} \leq \overline{P}_{r,n}\alpha_{r,s,t}; \quad \forall r \in R, \forall n \in N, \forall s \in S, \forall t \in T \tag{B.47}$$

For diesel power plants, the power generated must always be less than or equal to their capacity, as seen in Eq. (B.48), and the power difference between two consecutive hours must not exceed the maximum load shedding ramp, as shown in Eq. (B.49).

$$P_{g,n,s,t} \leq \overline{P}_{g,n}; \quad \forall g \in \{Oil\}, \forall n \in N, \forall s \in S, \forall t \in T \tag{B.48}$$

$$-R_g\overline{P}_{g,n} \leq P_{g,n,s,t-1} - P_{g,n,s,t} \leq R_g\overline{P}_{g,n}; \quad \forall g \in \{Oil\}, \forall n \in N, \forall s \in S, \forall t \in T \tag{B.49}$$

Eq. (B.50) shows the operating chart relating active and reactive power with capacities for each generator, using tangent lines to limit feasible regions for active and reactive power operating points for transmission line limits.

$$-\frac{-\alpha P_{g,n,s,t} + \overline{S}_{g,n}}{\sqrt{1-\alpha^2}} \leq Q_{g,n,s,t} \leq \frac{-\alpha P^{g}_{n,s,t} + \overline{S}_{g,n}}{\sqrt{1-\alpha^2}} \quad \forall \alpha \in (-1,1), \forall g \in G, \forall n \in N, \forall s \in S, \forall t \in T \tag{B.50}$$

The following equations show the batteries predetermined duration model. The charging and discharging power must be less than the batteries' powers (Eqs. (B.51) and (B.52)), and stored energy must not exceed the battery's capacity multiplied by charging duration (Eq. (B.53)).

$$P^{BS}_{n,s,t} = P^{BS-}_{n,s,t} - P^{BS+}_{n,s,t}; \quad \forall n \in N, \forall s \in S, \forall t \in T \tag{B.51}$$

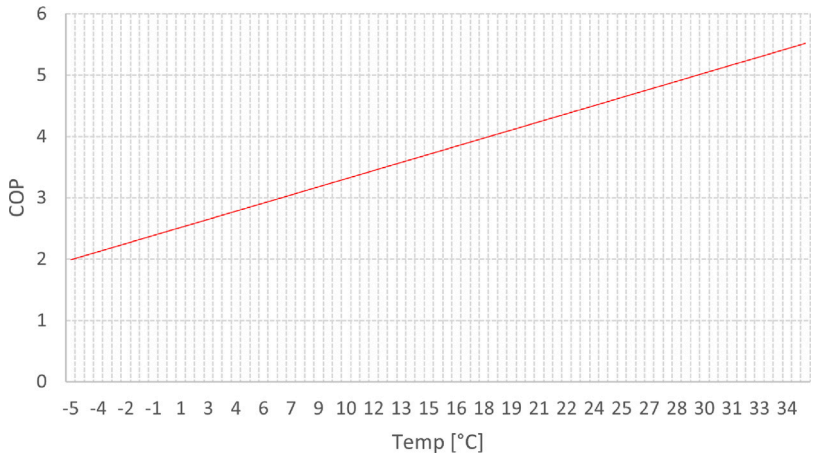

Fig. 16. Variation of COP with temperature [55].

$$-\overline{P}_n^{BS} \le P_{n,s,t}^{BS} \le \overline{P}_n^{BS}; \qquad \forall n \in N, \forall s \in S, \forall t \in T \tag{B.52}$$

$$P_{n,s,t}^{BSE} \le \overline{P}^{BS} \tau^{BS}; \qquad \forall n \in N, \forall s \in S, \forall t \in T \tag{B.53}$$

Charge states are coupled using an inventory constraint, Eq. (B.54), and the reactive power that can be injected by the battery is modelled in the same way as for generators (Eq. (B.55)).

$$P_{n,s,t}^{BSE} = P_{n,s,t-1}^{BSE} - P_{n,s,t}^{BS-} + P_{n,s,t}^{BS+}\eta^{BS}; \qquad \forall n \in N, \forall s \in S, \forall t \in T \tag{B.54}$$

$$-\frac{-\alpha P_{n,s,t}^{BS} + \overline{S}_n^{BS}}{\sqrt{1-\alpha^2}} \le Q_{n,s,t}^{BS} \le \frac{-\alpha P_{n,s,t}^{BS} + \overline{S}_n^{BS}}{\sqrt{1-\alpha^2}}; \quad \forall \alpha \in (-1,1), \forall n \in N, \forall s \in S, \forall t \in T \tag{B.55}$$

B.8. Following heat demand profile

The sum of heat outputs generated by the technologies connected to the district heating network must follow the heat demand profile (Eq. (B.56)). The same applies for end-user hydrogen boilers (Eq. (B.57)), and for the sum of outputs of residential heat pumps with auxiliary electric heaters (Eq. (B.58)). The profile to be followed by these three technology groups (district heat, hydrogen boilers, and heat-pump/auxiliary electric heater units) can be either the total heat demand profile, the domestic hot water profile, or the space-heating demand profile.

$$h_{p,n,t} \cdot \sum_{h\in\{HP,CHP,HB,HCHP\}} \overline{H}_{h,n} \le \sum_{h\in\{HP,CHP,HB,HCHP\}} H_{h,n,s,t}; \quad \forall p \in P, \forall n \in N, \forall s \in S, \forall t \in T \tag{B.56}$$

$$h_{p,n,t} \cdot \sum_{h\in\{EHB\}} \overline{H}_{h,n} \le \sum_{h\in\{EHB\}} H_{h,n,s,t}; \quad \forall p \in P, \forall n \in N, \forall s \in S, \forall t \in T \tag{B.57}$$

$$h_{p,n,t} \cdot \sum_{h\in\{Aux,ASHP\}} \overline{H}_{h,n} \le \sum_{h\in\{Aux,ASHP\}} H_{h,n,s,t}; \quad \forall p \in P, \forall n \in N, \forall s \in S, \forall t \in T \tag{B.58}$$

Firewood must follow space-heating demand profiles (Eq. (B.59)) and LPG technologies must follow water-heating demand profiles (Eq. (B.60)).

$$h_{p,n,t} \cdot \overline{H}_{h,n} \le H_{h,n,s,t}; \qquad \forall p \in \{HT\}, h \in \{FW\}, \forall n \in N, \forall s \in S, \forall t \in T \tag{B.59}$$

$$h_{p,n,t} \cdot \overline{H}_{h,n} \le H_{h,n,s,t}; \quad \forall p \in \{DHW\}, h \in \{LPG\}, \forall n \in N, \forall s \in S, \forall t \in T \tag{B.60}$$

Finally, firewood and LPG consumption cannot be higher than the current use as imposed by Eqs. (B.61) and (B.62), respectively.

$$H_{h,n,s,t} \le H_{n,t}^{DFW}; \qquad h \in \{FW\}, \forall n \in N, \forall s \in S, \forall t \in T \tag{B.61}$$

$$H_{h,n,s,t} \le H_{n,t}^{DLPG}; \qquad h \in \{LPG\}, \forall n \in N, \forall s \in S, \forall t \in T \tag{B.62}$$

B.9. Emission limits

Finally, Eq. (B.63) caps the total system's annual CO_2, while Eq. (B.64) limits particulate matter produced from firewood combustion.

$$\sum_{s\in S}\sum_{n\in N}\sum_{t\in T} \rho_s (P_{g=Oil,n,s,t} CE_{oil} + G_{n,s,t}^{LNG} CE_{LNG} + C_{n,s,t}^{LPG} CE_{LPG}) \le CET \tag{B.63}$$

$$\sum_{s\in S}\sum_{n\in N}\sum_{t\in T} \rho_s C_{n,s,t}^{FW} PM^{FW} \le PMT \tag{B.64}$$

Appendix C. Variation of the coefficient of performance with outside temperatures for air-source heat pumps

See Fig. 16.

Appendix D. Energy service demand profiles

See Figs. 17 and 18.

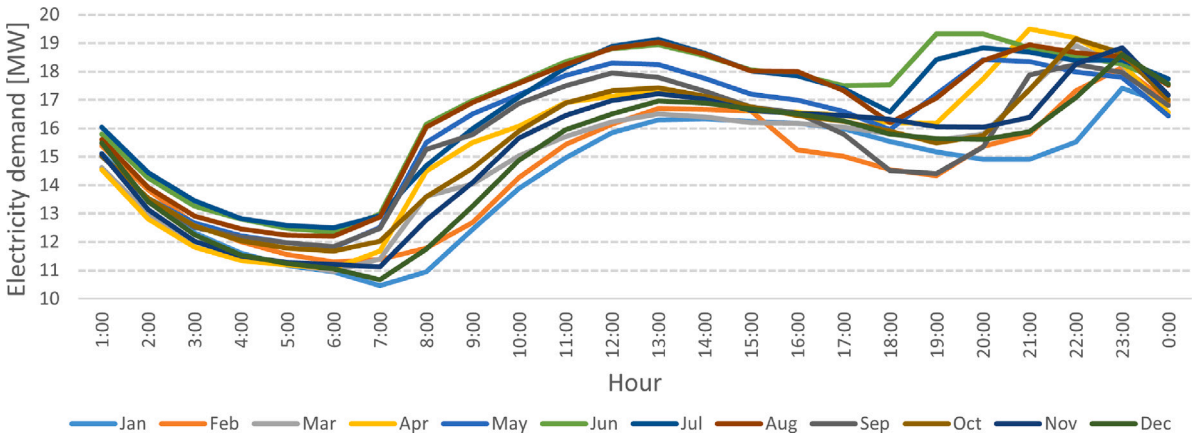

Fig. 17. Electricity demand profiles.

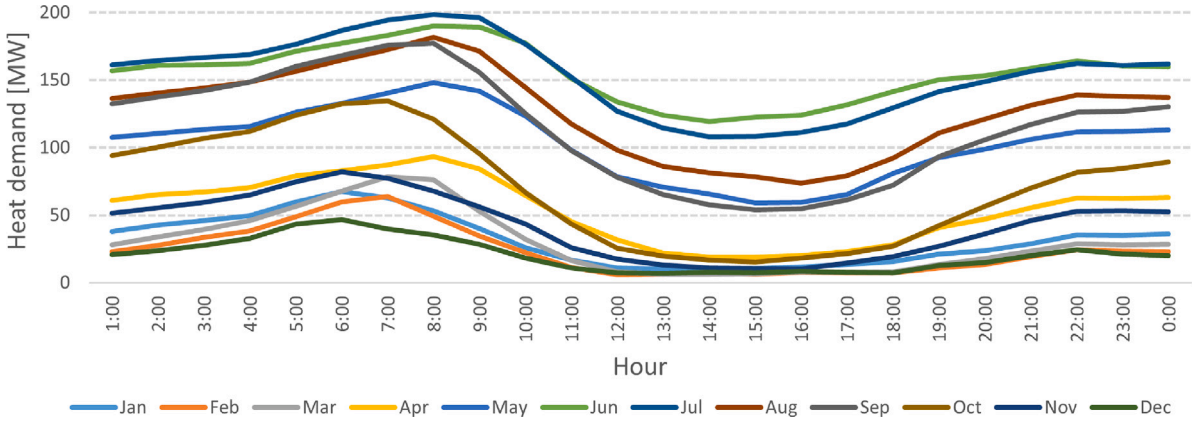

Fig. 18. Heat demand profiles.

References

[1] IPCC. Summary for policymakers. In: Masson-Delmotte V, Zhai P, Pirani A, Connors S, Péan C, Berger S, Caud N, Chen Y, Goldfarb L, Gomis M, Huang M, Leitzell K, Lonnoy E, Matthews J, Maycock T, Waterfield T, Yelekçi O, Yu R, Zhou B, editors. Climate change 2021: The Physical science basis. Contribution of working group I to the sixth assessment report of the intergovernmental panel on climate change. 2021, [in press].

[2] Hannah Ritchie MR, Rosado P. CO_2 and greenhouse gas emissions. 2020, Our World in Data https://ourworldindata.org/co2-and-other-greenhouse-gas-emissions.

[3] IQAir. World air quality report – region & city PM2.5 ranking. 2021.

[4] Comisión Nacional de Energía. Balance Nacional de Energía año 2019. 2019, Available online: http://energiaabierta.cl/visualizaciones/balance-de-energia/.

[5] Consejo de Ministros para la Sustentabilidad, Gobierno de Chile. Chile's nationally determined contribution, update 2020. 2020.

[6] Lovell K, Foxon TJ. Framing branching points for transition: Policy and pathways for UK heat decarbonisation. Environ Innov Soc Transitions 2021;40:147–58. http://dx.doi.org/10.1016/j.eist.2021.06.007, URL https://www.sciencedirect.com/science/article/pii/S2210422421000381.

[7] Lund H, Werner S, Wiltshire R, Svendsen S, Thorsen JE, Hvelplund F, et al. 4Th generation district heating (4GDH): Integrating smart thermal grids into future sustainable energy systems. Energy 2014;68:1–11. http://dx.doi.org/10.1016/j.energy.2014.02.089, URL https://www.sciencedirect.com/science/article/pii/S0360544214002369.

[8] Dodds PE, Staffell I, Hawkes AD, Li F, Grünewald P, McDowall W, et al. Hydrogen and fuel cell technologies for heating: A review. Int J Hydrogen Energy 2015;40(5):2065–83. http://dx.doi.org/10.1016/j.ijhydene.2014.11.059, URL https://www.sciencedirect.com/science/article/pii/S0360319914031383.

[9] Lepiksaar K, Mašatin V, Latõšov E, Siirde A, Volkova A. Improving CHP flexibility by integrating thermal energy storage and power-to-heat technologies into the energy system. Smart Energy 2021;2:100022. http://dx.doi.org/10.1016/j.segy.2021.100022, URL https://www.sciencedirect.com/science/article/pii/S2666955221000228.

[10] IEA. Renewables 2019. 2019, Available online: https://www.iea.org/reports/renewables-2019.

[11] Jradi M, Riffat S. Tri-generation systems: Energy policies, prime movers, cooling technologies, configurations and operation strategies. Renew Sustain Energy Rev 2014;32:396–415. http://dx.doi.org/10.1016/j.rser.2014.01.039, URL https://www.sciencedirect.com/science/article/pii/S1364032114000501.

[12] Mancarella P. MES (multi-energy systems): An overview of concepts and evaluation models. Energy 2014;65:1–17. http://dx.doi.org/10.1016/j.energy.2013.10.041, URL https://www.sciencedirect.com/science/article/pii/S0360544213008931.

[13] Capuder T, Mancarella P. Techno-economic and environmental modelling and optimization of flexible distributed multi-generation options. Energy 2014;71. http://dx.doi.org/10.1016/j.energy.2014.04.097.

[14] Strbac G. Demand side management: Benefits and challenges. Energy Policy 2008;36:4419–26. http://dx.doi.org/10.1016/j.enpol.2008.09.030.

[15] Zhang L, Good N, Mancarella P. Building-to-grid flexibility: Modelling and assessment metrics for residential demand response from heat pump aggregations. Appl Energy 2019;233–234:709–23. http://dx.doi.org/10.1016/j.apenergy.2018.10.058.

[16] Vijay A, Hawkes A. Demand side flexibility from residential heating to absorb surplus renewables in low carbon futures. Renew Energy 2019;138. http://dx.doi.org/10.1016/j.renene.2019.01.112.

[17] Mancarella P, Chicco G. Real-time demand response from energy shifting in distributed multi-generation. IEEE Trans Smart Grid 2013;4:1928–38. http://dx.doi.org/10.1109/TSG.2013.2258413.

[18] Liu X, Wu J, Jenkins N, Bagdanavicius A. Combined analysis of electricity and heat networks. Appl Energy 2016;162:1238–50. http://dx.doi.org/10.1016/j.apenergy.2015.01.102, URL https://www.sciencedirect.com/science/article/pii/S0306261915001385.

[19] Li G, Zhang R, Jiang T, Chen H, Bai L, Cui H, et al. Optimal dispatch strategy for integrated energy systems with CCHP and wind power. Appl Energy 2017;192:408–19. http://dx.doi.org/10.1016/j.apenergy.2016.08.139, URL https://www.sciencedirect.com/science/article/pii/S030626191631248X.

[20] van Beuzekom I, Hodge B-M, Slootweg H. Framework for optimization of long-term, multi-period investment planning of integrated urban energy systems. Appl Energy 2021;292:116880. http://dx.doi.org/10.1016/j.apenergy.2021.116880, URL https://www.sciencedirect.com/science/article/pii/S0306261921003664.

[21] Liu X, Mancarella P. Modelling, assessment and Sankey diagrams of integrated electricity-heat-gas networks in multi-vector district energy systems. Appl Energy 2016;167:336–52. http://dx.doi.org/10.1016/j.apenergy.2015.08.089, URL https://www.sciencedirect.com/science/article/pii/S0306261915010259.

[22] Martínez Ceseña EA, Mancarella P. Energy systems integration in smart districts: Robust optimisation of multi-energy flows in integrated electricity, heat and gas networks. IEEE Trans Smart Grid 2019;10(1):1122–31. http://dx.doi.org/10.1109/TSG.2018.2828146.

[23] Saint-Pierre A, Mancarella P. Integrated electricity and heat active network management. In: 2016 Power Systems Computation Conference. PSCC, 2016, p. 1–7. http://dx.doi.org/10.1109/PSCC.2016.7540998.

[24] Zhong X, Zhong W, Liu Y, Yang C, Xie S. Optimal energy management for multi-energy multi-microgrid networks considering carbon emission limitations. Energy 2022;246:123428. http://dx.doi.org/10.1016/j.energy.2022.123428, URL https://www.sciencedirect.com/science/article/pii/S0360544222003310.

[25] Martínez Ceseña EA, Capuder T, Mancarella P. Flexible distributed multienergy generation system expansion planning under uncertainty. IEEE Trans Smart Grid 2016;7(1):348–57. http://dx.doi.org/10.1109/TSG.2015.2411392.

[26] Berger M, Radu D, Fonteneau R, Deschuyteneer T, Detienne G, Ernst D. The role of power-to-gas and carbon capture technologies in cross-sector decarbonisation strategies. Electr Power Syst Res 2020;180:106039. http://dx.doi.org/10.1016/j.epsr.2019.106039, URL https://www.sciencedirect.com/science/article/pii/S037877961930358X.

[27] Jalil Vega F, Hawkes A. Spatially resolved optimization for studying the role of hydrogen for heat decarbonization pathways. ACS Sustain Chem Eng 2018;6. http://dx.doi.org/10.1021/acssuschemeng.7b03970.

[28] Jalil Vega F, Hawkes A. Spatially resolved model for studying decarbonisation pathways for heat supply and infrastructure trade-offs. Appl Energy 2017;210. http://dx.doi.org/10.1016/j.apenergy.2017.05.091.

[29] Fu P, Pudjianto D, Zhang X, Strbac G. Integration of hydrogen into multi-energy systems optimisation. Energies 2020;13(7). http://dx.doi.org/10.3390/en13071606, URL https://www.mdpi.com/1996-1073/13/7/1606.

[30] Estermann T, Newborough M, Sterner M. Power-to-gas systems for absorbing excess solar power in electricity distribution networks. Int J Hydrogen Energy 2016;41(32):13950–9. http://dx.doi.org/10.1016/j.ijhydene.2016.05.278, URL https://www.sciencedirect.com/science/article/pii/S0360319916317700.

[31] Clegg S, Mancarella P. Storing renewables in the gas network: modelling of power-to-gas seasonal storage flexibility in low-carbon power systems. IET Gener Transm Distrib 2016;10(3):566–75. http://dx.doi.org/10.1049/iet-gtd.2015.0439, arXiv:https://ietresearch.onlinelibrary.wiley.com/doi/pdf/10.1049/iet-gtd.2015.0439, URL https://ietresearch.onlinelibrary.wiley.com/doi/abs/10.1049/iet-gtd.2015.0439.

[32] Fu P, Pudjianto D, Strbac G. Integration of power-to-gas and low-carbon road transport in Great Britain's future energy system. IET Renew Power Gener 2021;14. http://dx.doi.org/10.1049/iet-rpg.2020.0595.

[33] Clegg S, Mancarella P. Integrated modeling and assessment of the operational impact of power-to-gas (P2G) on electrical and gas transmission networks. IEEE Trans Sustain Energy 2015;6(4):1234–44. http://dx.doi.org/10.1109/TSTE.2015.2424885.

[34] Petkov I, Gabrielli P. Power-to-hydrogen as seasonal energy storage: an uncertainty analysis for optimal design of low-carbon multi-energy systems. Appl Energy 2020;274:115197. http://dx.doi.org/10.1016/j.apenergy.2020.115197, URL https://www.sciencedirect.com/science/article/pii/S0306261920307091.

[35] Pan G, Gu W, Lu Y, Qiu H, Lu S, Yao S. Optimal planning for electricity-hydrogen integrated energy system considering power to hydrogen and heat and seasonal storage. IEEE Trans Sustain Energy 2020;11(4):2662–76. http://dx.doi.org/10.1109/TSTE.2020.2970078.

[36] Ghanbari A, Karimi H, Jadid S. Optimal planning and operation of multi-carrier networked microgrids considering multi-energy hubs in distribution networks. Energy 2020;204:117936. http://dx.doi.org/10.1016/j.energy.2020.117936, URL https://www.sciencedirect.com/science/article/pii/S0360544220310434.

[37] Boffino L, Conejo AJ, Sioshansi R, Oggioni G. A two-stage stochastic optimization planning framework to decarbonize deeply electric power systems. Energy Econ 2019;84:104457. http://dx.doi.org/10.1016/j.eneco.2019.07.017, URL https://www.sciencedirect.com/science/article/pii/S0140988319302385.

[38] Farivar M, Low SH. Branch flow model: Relaxations and convexification—Part I. IEEE Trans Power Syst 2013;28(3):2554–64. http://dx.doi.org/10.1109/TPWRS.2013.2255317.

[39] Moreno R, Moreira R, Strbac G. A MILP model for optimising multi-service portfolios of distributed energy storage. Appl Energy 2015;137:554–66. http://dx.doi.org/10.1016/j.apenergy.2014.08.080, URL https://www.sciencedirect.com/science/article/pii/S0306261914008915.

[40] Comisión Nacional de Energía. Informe técnico definitivo estudio de planificación y tarificación de los sistemas medianos de Aysén, Palena y General Carrera, Cuadrilenio 2018–2022. 2019, Disponible en línea: https://www.cne.cl/tarificacion/electrica/tarificacion-sistemas-medianos/.

[41] Corporación de Desarrollo Tecnológico. Medición del consumo nacional de leña y otros combustibles sólidos derivados de la madera, Disponible en línea: https://calefaccionsustentable.mma.gob.cl/wp-content/uploads/2017/09/Medicion-del-consumo-nacional-de-lena-y-otros-combustibles-solidos/-derivados-de-la-madera.pdf.

[42] Perez P, Menares C, Ramírez C. PM2.5 forecasting in Coyhaique, the most polluted city in the Americas. Urban Clim. 2020;32:100608. http://dx.doi.org/10.1016/j.uclim.2020.100608, URL https://www.sciencedirect.com/science/article/pii/S2212095519303207.

[43] Ministerio de Energía. Informe final de usos de la energía de los hogares en Chile. 2018, Disponible en línea: https://www.energia.gob.cl/sites/default/files/documentos/informe_final_caracterizacion_residencial_2018.pdf.

[44] Ministerio de Energía. Evaluación de proyectos de calefacción distrital para ciudad de Coyhaique y Puerto Williams. 2019, Disponible en línea: https://energia.gob.cl/educacion/energia-distrital.

[45] Ministerio de Medio Ambiente. Sistema de Información Nacional de Calidad del Aire, Disponible en línea: https://sinca.mma.gob.cl/index.php/estacion/index/id/238.

[46] Ministerio de Energía. Explorador Solar, Disponible en línea: https://solar.minenergia.cl.

[47] Ministerio de Energía. Explorador Eólico, Disponible en línea: https://eolico.minenergia.cl.

[48] Inzunza A, Muñoz FD, Moreno R. Measuring the effects of environmental policies on electricity markets risk. Energy Econ 2021;102:105470. http://dx.doi.org/10.1016/j.eneco.2021.105470, URL https://www.sciencedirect.com/science/article/pii/S014098832100356X.

[49] Ministerio de Energía. Informe de actualización de antecedentes. Planificación energética de largo plazo. 2019, Disponible en línea: https://energia.gob.cl/documentos/informes-de-actualizacion-de-antecedentes-pelp-2018-2022.

[50] Comisión Nacional de Energía. Estudio de Costos de Servicios Asociados al Suministro de Electricidad de Distribución. 2017, Disponible en línea: https://www.cne.cl/tarificacion/electrica/valor-agregado-de-distribucion/vad-2016-2020-y-servicios-asociados/.

[51] SEREMI de Energía Aysén. Reporte de leña certificada, Disponible en línea: https://https://energia.gob.cl/sites/default/files/lena_aysen_10_nov_2020.pdf.

[52] Houck JE, Broderick DR. PM2.5 emission reduction benefits of replacing conventional uncertified cordwood stoves with certified cordwood stoves or modern pellet stoves. OMNI Environmental Services, Inc., Prepared for Hearth, Patio and Barbecue Association; 2005.

[53] FICO Xpress Optimization. Disponible en línea: https://www.fico.com/en/products/fico-xpress-optimization.

[54] Ministerio de Medio Ambiente. Hoja de ruta de calefacción distrital para Chile. 2016, Disponible en línea: http://achbiom.cl/wp-content/uploads/2017/08/documento-hoja-de-ruta.pdf.

[55] Qadrdan M, Fazeli R, Jenkins N, Strbac G, Sansom R. Gas and electricity supply implications of decarbonising heat sector in GB. Energy 2019;169:50–60. http://dx.doi.org/10.1016/j.energy.2018.11.066, URL https://www.sciencedirect.com/science/article/pii/S0360544218322771.